# Direct Diabatization Based on Nonadiabatic Couplings: The N/D Method

**SCHOLARONE™**
Manuscripts

# Direct Diabatization Based on Nonadiabatic Couplings: The N/D Method

Zoltan Varga,[†] Kelsey A. Parker,[†] and Donald G. Truhlar*

*Department of Chemistry, Chemical Theory Center, and Minnesota Supercomputing Institute, 207 Pleasant Street SE, University of Minnesota, Minneapolis, MN 55455-0431*

Author information:

*Corresponding author: truhlar@umn.edu

†ZV and KAP contributed equally.

ORCID

Zoltan Varga: 0000-0002-9324-798X

Kelsey A. Parker: 0000-0002-9176-3681

Donald G. Truhlar: 0000-0002-7742-7294

**Abstract**

Diabatization converts adiabatic electronic states to diabatic states, which can be fit with smooth functions, thereby decreasing the computational time for simulations. Here we present a new diabatization scheme based on components of the nonadiabatic couplings and the adiabatic energy gradients. The nonadiabatic couplings are multi-dimensional vectors that are singular along conical intersection seams, and this makes them essentially impossible to fit; furthermore they have unphysical aspects due to the assumptions of the generalized Born-Oppenheimer scheme, and therefore they are not usually used in diabatization schemes. However, we show here that the nonadiabatic couplings can provide a route to obtaining diabatic states by using the sign change of the energy gradient differences of adiabatic states on paths through conical intersections or locally avoided crossings. We present examples applying the method successfully to several test systems. We compare the method to other diabatization methods previously developed in our group.

# 1. Introduction

Photodynamical processes are central to many applications in laser-driven chemistry, light-driven devices, biological chemistry, photocatalysis, and solar cells. Photodynamics can be calculated quantum mechanically in the electronically adiabatic representation or in a diabatic representation. Adiabatic electronic wave functions are solutions or approximate solutions of the electronic Schrödinger equation with fixed nuclei; in practice they diagonalize the electronic Hamiltonian in a basis of configuration state functions. In an adiabatic representation, electronic states are coupled by the action of the nuclear momentum and nuclear kinetic energy operators acting on the electronic wave functions; in semiclassical treatments one usually keeps only the nuclear momentum coupling, and the resulting vector coupling matrix elements are called nonadiabatic couplings (NACs).[1] The adiabatic representation is not appropriate if one wants to keep the dynamics cost low by using fitted potential energy surfaces and couplings because the adiabatic potential energy surfaces have cuspidal ridges along high-dimensional conical intersection seams and NACs that are singular on these seams,[1,2] and these functions are almost impossible to fit. This motivates the transformation to a diabatic representation where the surfaces and couplings are smooth and scalar. Because the NACs cannot be completely transformed away,[2] a diabatic representation is defined as one where the electronic wave functions are smooth enough that NACs – although not zero – may be neglected; electronic transitions are then caused by off-diagonal elements of the electronic Hamiltonian, which is smooth but not diagonal in a diabatic representation. The off-diagonal elements of the electronic Hamiltonian are called diabatic couplings (DCs).[1,2]

For dynamics calculations, it is computationally efficient to fit the potentials (i.e., potential energy functions) and state couplings to analytic functions. Although adiabatic potentials have the advantage that they may be calculated directly by standard electronic structure methods (such as variational methods, perturbation theory, coupled cluster theory, and density functional theory), they have the disadvantage, as mentioned above, that they cannot be fit. The diabatic surfaces can be fit with analytical functions, but they can't be calculated directly by standard (variational) electronic structure methods. To address these limitations, we are interested in a process called diabatization, which is a way to switch from the adiabatic to the diabatic representation. Diabatic transformations have been widely studied dating back to seminal work by Lichten,[3] Smith,[4] and O'Malley.[5] Approximate diabatic representations may be based on smooth electronic wave functions like valence bond states, but in general one must find a mathematical scheme that uncovers the underlying smooth electronic states while retaining the accuracy achievable with adiabatic representations. Many diabatization methods have been developed, but work continues with the goal of designing a generally applicable, easy-to-use, and low-cost method.

Diabatization methods may be classified in various ways. One classification is into direct and indirect. Direct diabatization[6,7,8,9,10,11,12,13,14,15] (also referred to as point-by-point diabatization) can be accomplished at a given geometry without following a path to that geometry; indirect diabatizations[16,17,18] involve making the diabatic potential functions or wave functions smooth with respect to a previous point on a path. Direct diabatizations are preferred because it is hard to guarantee that path-dependent methods are independent of the path taken and because it is very laborious to cover all space with a set of paths.

Another classification is into orbital-dependent and orbital-independent. Orbital-dependent diabatizations[7,8,9,10,11,12,17,18] start by finding a set of smoothly varying orbitals called diabatic molecular orbitals (DMOs), which usually include reference orbitals. (Canonical molecular orbitals have avoided crossings and are therefore not smooth.) Diabatic molecular orbitals can be used to define diabatic state functions, and diabatic states can be defined in term of these by configurational uniformity.[7,8,9,10,11,12] Orbital-free diabatizations[6,13,14,15] avoid the need to find DMOs, which is an advantage because the definition of reference orbitals may require system-specific expertise or trail-and-error.

A third classification of diabatization methods is into adiabatic-equivalent[6,7,8,9,10,11,12,13,14,15,16,17,18] and adiabatic-nonequivalent[19,20]. A set of adiabatic-equivalent diabatic states spans the same space as a chosen set of adiabatic states, whereas a set of adiabatic non-equivalent diabats does not. For example, a set of valence bond states is smooth and might form a useful set of diabatic states, but it is obtained independently of any set of adiabatic states.[19] The advantage of adiabatic-equivalent diabatic states is that one obtains the original set of adiabatic potential energy surfaces by diagonalizing the diabatic Hamiltonian matrix.

Adiabatic potential energy surfaces intersect on $(F-2)$-dimensional seams called conical intersections, where $F$ is the number of internal degrees of freedom. If one has $N$ atoms, then $F = 3N - 6$. Passing through a conical intersection seam corresponds to crossing cuspidal ridges on the adiabatic potential energy surfaces of the crossing states, i.e., the potentials are continuous with discontinuous derivatives. The NACs are $3N$-dimensional in atomic Cartesian coordinates, with each NAC being an element of an $n \times n$ anti-Hermitian matrix, and the NACs are singular on the cuspidal ridges. Since the cuspidal ridges are not necessarily determined by symmetry, the adiabatic potential energy surfaces and the NACs are essentially impossible to fit to functions. In general, trajectories do not pass precisely through conical intersections; they pass them at a finite distance away. In passing on the side of an intersection, the gap between two adiabatic surfaces goes through a local minimum, and we call the point of the local minimum a locally avoided crossing (the adiabatic surfaces, considered more globally, do cross on the conical intersection seam, even if they do not cross along a path – most paths do not pass precisely though the seam since it has a dimensionality two less than the full dimensionality of the internal coordinate

4

space). At a locally avoided crossing, if it is close to the conical intersection seam, both the adiabatic potential surfaces and the NACs may change rapidly, i.e., they are not smooth.

The elements of the diabatic Hamiltonian should be smooth at conical intersections and locally avoided crossings. Another advantage of the diabatic representation is that there is no complication due to geometric phase.[21] When the diabatic Hamiltonian has been determined as a function of geometry, one may fit each element to a smooth analytic function to enable efficient dynamics calculations, which may then be carried out in either the adiabatic or diabatic representation. In the adiabatic case, one keeps only the nonadiabatic coupling that comes from the diabatic-to-adiabatic transformation. This is easy to calculate from the diabatic analytic functions on the fly without facing the task of fitting singular high-dimensional NAC vectors at cuspidal ridges (one only fits the smooth low-dimensional scalar diabatic Hamiltonian matrices).

In previous work we have used the fourfold way[9,10,11,12] and the dipole, quadrupole, and electrostatic potential (DQΦ) method[14,15] for diabatization. Both methods are direct and adiabatic-equivalent, and neither requires the calculation of electronic structure NACs; the fourfold way is orbital-dependent and the DQΦ method is orbital-free. Here we propose a new direct, adiabatic-equivalent, orbital-free diabatization scheme that uses the electronic structure NACs in the first step.

## 2. Theory

### 2.1. Transformation

As described in the Introduction, in an adiabatic representation, the NACs arise from the nuclear momentum and nuclear kinetic energy operators acting on the electronic wave functions.[1,2] The nonrelativistic, spin-free Schrödinger equation can be written as[1]:

$$\left\{ -\frac{1}{2\mu} \nabla_{\mathbf{R}}^2 + \widehat{H}_{el}(\mathbf{R}, \mathbf{r}) \right\} \Psi(\mathbf{R}, \mathbf{r}) = E\Psi(\mathbf{R}, \mathbf{r}) \tag{1}$$

where $E$ is the total energy, the electronic coordinates are denoted by $\mathbf{r}$, the nuclear coordinates by $\mathbf{R}$, and the nuclear mass by $\mu$. (We use isoinertial coordinates so masses are the same for all nuclei.) The electronic Hamiltonian, which includes electronic kinetic energy, electron-electron, electron-nuclear, and nuclear-nuclear interactions, is denoted by $H_{el}$, the Laplacian ($\nabla_R^2$) extends over all nuclear coordinates, and $\Psi(R, r)$ is the wave function. The wave function can be expanded as[1]:

$$\Psi(\mathbf{R}, \mathbf{r}) = \sum_{j=1}^{n} \psi_j(\mathbf{R}) \phi_j(\mathbf{r}; \mathbf{R}) \tag{2}$$

where $j$ labels electronic states, $\phi_j(\mathbf{r}; \mathbf{R})$ are normalized eigenfunctions of the electronic Hamiltonian, and $\psi_j(R)$ are nuclear wave functions. Substituting eqn (2) into eqn (1) yields,[1]

$$\left\{ -\frac{1}{2\mu} \nabla_{\mathbf{R}}^2 + V_j(\mathbf{R}) \right\} \psi_j(\mathbf{R}) + \sum_k \left\{ -\frac{1}{\mu} \vec{f}_{jk}(\mathbf{R}) \cdot \nabla_{\mathbf{R}} - \frac{1}{2\mu} t_{jk}(\mathbf{R}) \right\} \psi_k(\mathbf{R}) = E\psi_j(\mathbf{R}) \tag{3}$$

where

$$V_j(\mathbf{R}) = \int \phi_j^*(\boldsymbol{r}; \boldsymbol{R}) \hat{H}_{el}\, \phi_j(\boldsymbol{r}; \boldsymbol{R}) d\boldsymbol{r} \tag{4}$$

$$\vec{f}_{jk}(\mathbf{R}) = \int \phi_j^*(\boldsymbol{r}; \boldsymbol{R}) \nabla_R\, \phi_k(\boldsymbol{r}; \boldsymbol{R}) d\boldsymbol{r} \tag{5}$$

$$t_{jk}(\mathbf{R}) = \int \phi_j^*(\boldsymbol{r}; \boldsymbol{R}) \nabla_R^2\, \phi_k(\boldsymbol{r}; \boldsymbol{R}) d\boldsymbol{r} \tag{6}$$

The function $V_j(\boldsymbol{R})$, is the adiabatic potential energy function for nuclear motion in state $j$, and these potentials may be assembled as the elements of a diagonal matrix $\mathbf{V}(\mathbf{R})$. We always arrange them such that $V_1(\boldsymbol{R}) \leq V_2(\boldsymbol{R}) \leq V_3(\boldsymbol{R})$ .... For $N$ atoms, the vector $\vec{f}_{jk}(\mathbf{R})$ is the $3N$-dimensional nuclear momentum coupling vector between states $j$ and $k$, and $t_{jk}(\mathbf{R})$ is the kinetic energy coupling, which is usually considered less important in semiclassical approximations,[22] and which can also be hard to treat consistently in approximate approaches.[23] (We omit it here not because it is necessarily ignorable but rather as part of the freedom we have to choose a non-unique diabatic transformation.) In the rest of the paper, $\vec{f}_{jk}(\mathbf{R})$ will be called a NAC. Note that a NAC is a $3N$-dimensional vector in coordinate space, but it is also an off-diagonal matrix element of an $n \times n$ matrix in electronic state space; the anti-Hermitian property of the gradient in eqn (5) means that[1]

$$\vec{f}_{jk}(\mathbf{R}) = -\vec{f}_{kj}(\mathbf{R}) \tag{7}$$

and

$$\vec{f}_{jj}(\mathbf{R}) = 0 \tag{8}$$

In a diabatic representation, one neglects the NACs.[1,2] Although it is well known that one cannot completely eliminate the coupling due to NACs,[2] the idea of making a transformation with a form similar to diagonalizing the NAC matrix is what motivates our strategy. In particular, we obtain a diabatic representation by a sequence of diagonalizations applied to matrices of the form:

$$\mathbf{M}^{(jk)}(\mathbf{R}) = \begin{bmatrix} M_j^{(jk)}(\mathbf{R}) & f_{jk}(\mathbf{R}) \\ f_{jk}(\mathbf{R}) & M_k^{(jk)}(\mathbf{R}) \end{bmatrix}$$

where $f_{jk}(\mathbf{R})$ is the magnitude of $\vec{f}_{jk}(\mathbf{R})$. Because $\mathbf{M}^{(jk)}(\mathbf{R})$ is a symmetric $2 \times 2$ matrix, it can be diagonalized by a single Jacobi rotation,[24] which yields the diagonal matrix

$$\widetilde{\mathbf{M}}^{(jk)}(\mathbf{R}) = \left[\mathbf{P}^{(jk)}(\mathbf{R})\right]^{-1} \mathbf{M}^{(jk)}(\mathbf{R}) \mathbf{P}^{(jk)}(\mathbf{R}) \tag{9}$$

where

$$\mathbf{P}^{(jk)}(\mathbf{R}) = \begin{pmatrix} \cos\theta_{jk}(\boldsymbol{R}) & -\sin\theta_{jk}(\boldsymbol{R}) \\ \sin\theta_{jk}(\boldsymbol{R}) & \cos\theta_{jk}(\boldsymbol{R}) \end{pmatrix} \tag{10}$$

and where

6

$$\tan(2\theta_{jk}) = \frac{N_{jk}(\mathbf{R})}{D_{jk}(\mathbf{R})} \tag{11}$$

which will make the transformed off-diagonal $N_{jk}(\mathbf{R})$ element become zero in matrix $\widetilde{\mathbf{M}}^{(jk)}$.

The numerator is

$$N_{jk}(\mathbf{R}) = \tilde{f}_{jk}(\mathbf{R}) \tag{12}$$

with $\tilde{f}_{jk}(\mathbf{R})$ being either a NAC or a modified NAC, and the denominator is

$$D_{jk}(\mathbf{R}) = M_k^{(jk)}(\mathbf{R}) - M_j^{(jk)}(\mathbf{R}) \tag{13}$$

where $M_k^{(jk)}$ is explained in Section 2.3. The use of a modified NAC in the numerator allows us to remove undesired couplings in the Born–Oppenheimer approximation and will be explained in Section 2.2.

The rotation does not yield wave functions; the submatrix diagonalized is not a submatrix of the Hamiltonian. The resulting rotation angle $\theta_{jk}$ is then used for a 2×2 rotation of a submatrix of the Hamiltonian, which yields a continuous Hermitian diabatic Hamiltonian. Diagonalization of the diabatic Hamiltonian yields the original adiabatic eigenenergies.

When there are more than 2 states, we apply this transformation in sequence to "eliminate" NACs one-by-one; for example for 3-state case, first $f_{12}(\mathbf{R})$, then $f_{13}(\mathbf{R})$, and finally $f_{23}(\mathbf{R})$. Note that a Jacobi transformation makes previously rotated off-diagonal elements nonzero again, therefore the procedure has to be repeated until all of the off-diagonal elements become zero to within a pre-established tolerance. We stop the iteration if the root mean square of the off-diagonal elements is less than 5×10$^{-7}$ a. u. This sequence of transformations of the adiabatic basis functions is then used to transform the potential energy matrix into the diabatic representation. In particular, we get the following diabatic potential energy matrix:

$$[\mathbf{P}(\mathbf{R})]^{-1}\mathbf{V}(\mathbf{R})\mathbf{P}(\mathbf{R}) = \mathbf{U}(\mathbf{R}) \tag{14}$$

where $\mathbf{P}(\mathbf{R}) = \prod \mathbf{P}^{(jk)}(\mathbf{R})$, i.e., the product of the individual rotation matrices of state pairs.

After the transformation, rows and columns of $\mathbf{U}(\mathbf{R})$ correspond to the diabatic states, but they might not be in the right order. We found, however, that it is easy to re-order them by inspection.

The adiabatic potential curves or potential surfaces are sometimes called adiabats, and the diabatic potential curves or diabatic potential surfaces are sometimes called diabats.

The resulting method is called the N/D method to recognize the key role of eqn (11). All that remains is to identify suitable formulas for the numerator $N_{jk}(\mathbf{R})$ and the denominator $D_{jk}(\mathbf{R})$, that is, for $\tilde{f}_{jk}(\mathbf{R})$ and for $M_i^{(jk)}(\mathbf{R})$, with $i = j$ or $k$.

## 2.2. Numerator

First we consider the numerator. It is well documented that NACs are unphysical in various respects; this is discussed in various ways, including the lack of electron momentum in the Born-Oppenheimer basis and the dependence of conventional Born-Oppenheimer calculations on the coordinate system.[25,26,27,28,29,30,31,32,33,34,35,36,37,38,39,40,41,42,43,44] This is not a serious problem in regions where adiabatic states are strongly coupled because the NACs are singular at conical intersections and the singular terms that dominate in strongly coupled regions are free of these defects;[45] however, the incorrect behavior of NACs when subsystems separate is very inconvenient for dynamics.[25,26,28,32,33,40,43,44] Our first modification of NACs is to remove these long-range couplings because they are "fictitious" forces in the sense defined by Delos.[32] As in other aspects of the present treatment, we do this by taking advantage of the fact that diabatic states are not uniquely defined.

The starting NACs for the treatment proposed here are those calculated analytically by the *Molpro* electronic structure package.[46,47] These NACs are calculated by displacing one coordinate at a time in the $3N$-dimensional Cartesian coordinate system without transformation to a center-of-mass coordinate system. These NACs may be written,

$$\vec{f}_{jk}(\mathbf{R}) = \sum_{\rho=1}^{N} \sum_{\gamma=1}^{3} f_{jk,\rho\gamma}(\mathbf{R})\hat{e}_{\rho\gamma} \tag{15}$$

where $\hat{e}_{\rho\gamma}$ is a unit vector, $\rho$ labels an atom in the $N$-atom system, $\gamma = 1,2,3$ corresponds to the $x,y,z$ Cartesian coordinates, and

$$f_{jk,\rho\gamma}(\mathbf{R}) = \int \phi_j^*(\mathbf{R},r)\frac{\partial}{\partial X_{\rho\gamma}}\phi_k(\mathbf{R},r)dr \tag{16}$$

where $X_{\rho\gamma}$ is an atomic Cartesian coordinate. To eliminate unphysical coupling we replace $\vec{f}_{jk}(\mathbf{R})$ by

$$\vec{g}_{jk}(\mathbf{R}) = \sum_{\rho=1}^{N} \sum_{\gamma=1}^{3} w_\rho f_{jk,\rho\gamma}(\mathbf{R})\hat{e}_{\rho\gamma} \tag{17}$$

where $w_\rho$ is a weighting function that may be different for each atom $\rho$ and may even be zero for some atoms, and we define

$$g_{jk}(\mathbf{R}) = |\vec{g}_{jk}(\mathbf{R})| \tag{18}$$

The choice to use the magnitudes of the NACs is well adapted to practical calculations because it is hard choose all the sign convention in practical electronic structure calculations to make the sign be a continuous function of geometry.

Our second modification is to place a threshold on the usage of the NACs. This serves two purposes: (i) it avoids unnecessary operations in regions where the NACs are very small and inconsequential and may be sensitive to the numerical methods used to compute them; (ii) it allows for stable treatment of asymptotic regions where the couplings should have no effect. Applying the threshold yields the following expression for the numerator:

$$N_{jk}(\mathbf{R}) \equiv \tilde{f}_{jk}(\mathbf{R}) = \begin{cases} 0 & \text{if } g_{jk} \leq f_{\text{thr}} \\ g_{jk}(\mathbf{R}) - f_{\text{thr}} & \text{otherwise} \end{cases} \tag{19}$$

where $f_{\text{thr},jk}$ is a parameter. If $\tilde{f}_{jk}(\mathbf{R})$ is zero and the dominator is positive (see in Section 2.3.) at some $\mathbf{R}$, then the diagonalization is skipped at that $\mathbf{R}$, i.e., $\mathbf{P}^{(jk)}(\mathbf{R})$ is set equal to the unit matrix ($\theta_{jk} = 0$ degrees), and no rotation of state $j$ with state $k$ occurs at that $\mathbf{R}$. If $\tilde{f}_{jk}(\mathbf{R})$ is zero and the dominator is negative at some $\mathbf{R}$, then a full rotation is applied ($\theta_{jk} = 90$ degrees), i.e., state $j$ and $k$ switch at geometry $\mathbf{R}$. In this way, the diabats are set equal to the adiabats in a way that is consistent with the rest of the surface.

In some cases, one might want to use a different weight or a different threshold for different state pairs (replace $w_\rho$ and/or $f_{\text{thr}}$ by $w_{jk,\rho}$ and/or $f_{\text{thr},jk}$), but that was not necessary here.

**2.3. Denominator**

The denominator needs to work in concert with the NACs to provide diabatic curves that have the correct physics. The proposed function for the denominator is

$$D_{jk}(\mathbf{R}) = \varepsilon \sum_{\rho=1}^{N-1} \sum_{\rho'=\rho+1}^{N} W_{jk,\rho\rho'} h_{jk,\rho\rho'}(\mathbf{R}) \tag{20}$$

where $\varepsilon$ is a scaling factor, $W_{jk,\rho\rho'}$ is a weight, and

$$h_{jk,\rho\rho'}(\mathbf{R}) = \frac{\partial}{\partial Q_{\rho\rho'}}\left[V_k(\mathbf{R}) - V_j(\mathbf{R})\right] \tag{21}$$

where $Q_{\rho\rho'}$ are the $N(N-1)/2$ internuclear distances of atom pairs $\rho$ and $\rho'$ for the $N$-atom system. Ideally, the internuclear distances that are roughly perpendicular to the seam of diabatic crossing should be used. This can be controlled by the weighting function $W_{jk,\rho\rho'}$ for each state pair. Notice that for $N > 4$, the internuclear distances are a redundant set of internal coordinates, but in practice we will set the weighting function of many of the partial derivatives equal to zero using $W_{jk,\rho\rho'}$, and the number of terms retained in eqn (20) will be less than $F$.

To motivate eqn (20), let's consider passing through a locally avoided intersection of two states of the same symmetry. In the diabatic representation, the two states cross, and the gradients of those two states are smooth and do not cross. In the adiabatic representation, the potential energy surfaces do not cross, but the two energy gradients must switch if those two adiabatic states have a crossing or avoided crossing due to a change in configuration. Therefore, the denominator will change sign, and therefore the tangent of eqn (11) will also change sign. On one side of the sign change, $2\theta_{jk}$ will be in the range 0 to $\pi/2$, and on the other side of the sign change it will be in the range $\pi/2$ to $\pi$. Consequently, on one side of the sign change, $\cos\theta_{jk}$ will be greater than $\sin\theta_{jk}$, but on the other side it will be smaller. Thus, the transformation of eqn (10) will switch the diabats from one adiabat to another, which is our goal. In a simple case a single $Q_{\rho\rho'}$ might be enough for diabatization.

According to eqn (20), a scaling factor ($\varepsilon$) is required to adjust the relative scale of the numerator and denominator because they would otherwise have different units. If the scaling factor were too small, then the nominator in eqn (11) will dominate, thus strong mixing would occur over a wide range of geometries. In an extreme case, the diabatic states would be stuck together instead of crossing one another. Even in the regions where the diabatic energies should be approximately equal to the adiabatic energies, the diabatic energies would still correspond to significant mixtures of adiabatic energies. On the other hand, if the scaling factor were too large, then the denominator in eqn (11) would dominate, and the diabatic coupling would be significant only for a very narrow range of geometries. In an extreme case, the diabatic energies would be approximately equal to the adiabatic energies, and due to the sign change the two diabatic curves would suddenly switch at the diabatic state crossing. A reasonable choice for $\varepsilon$ will result in a reasonable peak in the NAC. (Theoretically a NAC will approach infinity at a conical intersection; however, the usual case encountered for a polyatomic system along a path is a locally avoided crossing because it is unlikely that a path goes precisely through a conical intersection by chance).

If the diabatic crossing seam is highly curved, the employed coordinates $Q_{\rho\rho'}$ might need to be functions of $\mathbf{R}$ controlled by geometry-dependent $W_{jk,\rho\rho'}$, but $W_{jk,\rho\rho'}$ should be a smooth function. In our present treatment, we take $W_{jk,\rho\rho'}$ to be independent of geometry.

Recently, in a series of articles, Yarkony and coworkers have drawn attention to a potential problem of many diabatization techniques, an issue Yarkony calls diabolical seams.[48,49,50,51] When using a property-based diabatization method, one will often seek to find extremes of a function derived with adiabatic functions via the diagonalization of a matrix of adiabatic properties. Analogous to diagonalization of the Hamiltonian, diagonalization of the property matrix results in problematic seams along discontinuous derivatives. When one diagonalizes the Hamiltonian, there is an (F-2)-dimensional seam where the eigenvectors (adiabatic state functions) have discontinuous derivatives, and this is the seam of the conical intersections. When one diagonalizes the property matrix, there is an (F-2)-dimensional seam where the eigenvectors (diabatic state functions) have a discontinuous derivative and this is the seam of the diabolical singularities. This seam will occur when: $N_{jk}(\mathbf{R}) = D_{jk}(\mathbf{R}) = 0$ in our matrix component notation. This unwanted behavior can potentially be avoided by moving the DSs, via property selection, into regions of the surface that are not important in dynamics simulations. As we will show in the sections below, we did not encounter diabolical seams in our work.

In the following sections, we will show that the NACs and gradients of the adiabatic states, when used together, can provide relevant chemical insight into the system by uncovering the physical diabatic states that underlie the adiabatic ones.

# 3. Electronic structure methods

All of the calculations in this work were carried out using the *Molpro* program package[46,47] with state-averaged CASSCF,[52,53,54,55,56] i.e., SA($n$)-CASSCF, where $n$ is the number of states averaged. In all cases, equal weights were used for the state average. *Molpro* calculates the energy gradients for each state and the NAC values for the state couplings analytically via coupled-perturbed multi-configurational self-consistent field (MCSCF) calculations. active spaces will be labeled ($e,o$), where $e$ is the number of active electrons and $o$ is the number of active orbitals.

## 3.1. LiF

For the calculation of LiF dissociation, $C_{2v}$ symmetry was used and the first two singlet $A_1$ states were averaged with equal weights ($n = 2$). The 1s orbital of Li and the 1s and 2s orbitals of F were kept doubly occupied. The active space was (6,7), and the 6-311+G* basis set[57,58] was used. The potential energy curve was scanned from 0.8 Å to 10.0 Å.

## 3.2. H$_3$

Three sets of calculations were carried out for the H$_3$ system

The first set (called H$_3$-MEP) is along an approximate minimum energy path of H + H$_2$, where we note that geometries along this path are collinear. Three states were averaged, but only the first two singlet $A'$ states were used in the diabatization process ($n = 3$ for SA($n$)-CASSCF, but $n = 2$ for eqn (2)). The symmetry of the system was set to $C_s$. The active space was (3,15) with twelve $a'$ and three $a''$ orbitals; the def2-QZVP basis set[59] was used.

In the second set (called H$_3$-LIN), the arrangement of the three H atoms is set to be linear, then both $R_{12}$ and $R_{13}$ are changed from 1 to 6 bohr, with 0.2 bohr increments, to obtain the points of a two-dimensional (2D) surface ($R_{23} = R_{12} + R_{13}$). In this case, these calculations were carried out by using SA(2)-CASSCF(3,15)/def2-QZVP with $C_s$ symmetry. Note that the path of the H$_3$-MEP set, is the minimum-energy path through this this 2D surface.

The third set (called H$_3$-BENT) is again a 2D surface. The bond angle of H$_3$ fixed at 60 degrees, and both $R_{12}$ and $R_{13}$ are varied from 1 to 3 bohr with 0.1 bohr increments. In these calculations, SA(2)-CASSCF(3,15)/def2-QZVP was also used with $C_s$ symmetry.

## 3.3. (H$_2$)$_2$

The calculation of the H$_2$ dimer system corresponds to the calculation used in the previous fourfold way and DQΦ work.[9,15] Thus $n = 3$ in SA($n$)-CASSCF calculations, the active space is (4,4); and the TZP basis set[60] was used. The symmetry was turned off.

## 3.4. Li + HF

The reaction path of Li + FH → LiF + H was previously studied with the fourfold way and DQΦ method.[9,15] The symmetry of this three-body system is $C_s$. We consider $n = 2$ with both

states being singlet $A'$. The active space is (7,8), including the $2s$ and $2p$ orbitals of Li, the $2p$ orbitals of F, and the $1s$ orbital of H; the 6-311+G* basis set[57,58] was used.

### 3.5. PhOH

The photodissociation of phenol into PhO and H was also calculated. To get the diabatic representation for photodissociation, we considered $n = 3$. We used the same active space as Ref. 12, which is (12,11); the def2-SVPD basis set[61] was used. The equilibrium geometry of phenol was taken from Ref. 12. The torsion angle between the C(6)-C(1)-C(2) plane and the C(1)-O-H plane was $\theta = 45°$; therefore the calculated structures belong to $C_1$ symmetry. Then the OH bond distance was varied between 1.0 and 3.0 Å, and except for this bond distance and $\theta$, the other internal coordinates are fixed at their equilibrium values.

### 3.6. O₃

For $O_3$, $C_s$ symmetry was applied, and the first three $^3A'$ triplet states were calculated ($n = 3$). The active space was (12,9) including the nine 2p orbitals. The bond angle of the three oxygen atoms was fixed at 175 degrees. One of the bond lengths was fixed at the equilibrium distance of $O_2$ molecule, $R_e = 1.208$ Å, and the other bond length was scanned from 3 to 1 Å. In these calculations, the maug-cc-pVTZ basis set[62,63,64,65] was used.

In all the calculations described so far, the adiabatic states are obtained with SA($n$)-CASSCF and diabatization was carried out by the N/D method. For $O_3$, for comparison, we also ran calculations with the DQΦ method.[15] In the DQΦ calculations, we started with the same SA(3)-CASSCF(12,9) calculations as used for N/D and then added external correlation by extended multi-state second order perturbation theory[66,67,68,69] (XMS(3)-CASPT2) to obtain the adiabatic energies and dipole, quadruple, and electrostatic potential matrix elements required for DQΦ diabatization. The def2-TZVPD basis set[61] was used in the DQΦ calculations.

## 4. Applications

To apply the method to a given case, we must specify the options that can be different for different applications. There are four of these: (i) the unitless weights $w_\rho$ used in the numberator, (ii) the threshold $f_{thr}$ used in the numerator, (iii) the choices of internuclear distances $Q_{\rho\rho'}$ for each $jk$ state pair for the denominator as determined by the nonzero weights $W_{jk,\rho\rho'}$ used in the denonimator, and (iv) the energetic scaling parameter $\varepsilon$ used in the denominator. The values of these parameters used for the current article are given in Table 1.

**Table 1** Parameters of the N/D calculations$^a$

| System | $w_\rho$ | $f_{thr}$ $(a_0^{-1})$ | $\varepsilon$ $(E_h^{-1})$ | $W_{jk,\rho\rho'}$ |
|---|---|---|---|---|
| LiF | 1 | 0 | 160 | $W_{12,LiF} = 1$ |
| $H_3$-MEP | 1 | 0 | sets 1,2: 20 <br> set 3: 10 | set 1: $W_{12,12} = 1$ <br> set 2: $W_{12,13} = 1$ <br> set 3: $W_{12,12} = 1$, $W_{12,13} = -1$ |
| $H_3$-LIN | 1 | 0.2 | 10 | $W_{12,12} = 1$, $W_{12,13} = -1$ |
| $H_3$-BENT | 1 | 0.2 | 10 | $W_{12,12} = 1$, $W_{12,13} = -1$ |
| $(H_2)_2$ | 1 | 0 | 200 | set 1: $W_{23,12} = W_{23,13} = W_{23,23} = 1$ <br> $\quad\quad W_{23,14} = W_{23,24} = W_{23,34} = -1$ <br> set 2: $W_{jk,12} = W_{jk,13} = 1$ <br> $\quad\quad W_{jk,24} = W_{jk,34} = -1$ |
| LiHF | 1 | sets 1,3: 0.25 <br> set 2: 0.3 | sets 1,3: 70 <br> set 2: 300 | set 1: $W_{12,FH} = 1$ <br> set 2: $W_{12,LiF} = 1$ <br> set 3: $W_{12,LiF} = W_{12,LiH} = 1$ <br> $\quad\quad W_{12,FH} = -1$ |
| phenol | $w_{OH} = 1$ <br> $w_{other\,\rho} = 0$ | 0.2 | 80 | $W_{jk,OH} = 1$ |
| $O_3$ | 1 | 0.2 | 40 | $W_{jk,12} = 1$ <br> $W_{jk,13} = -1$ |

$^a$ 1 $a_0$ = 1 bohr = 0.5292 Å; 1 $E_h$ = 1 hartree = 27.212 eV. The value of $w_\rho$ is the same for all $\rho$ except where indicated otherwise. Only nonzero $W_{jk,\rho\rho'}$ are shown.

In the application of N/D method, the choices of NAC (nominator) and adiabatic energy gradient (denominator) are system dependent as listed in Table 1. These system-dependent choices provide some freedom to avoid diabolical singularities, where $N_{jk}(\mathbf{R}) = D_{jk}(\mathbf{R}) = 0$. By using well chosen parameters, one can move the diabolical singularities to a region of the surface that is unimportant for the dynamics of interest.

## 4.1 LiF

Our first example is LiF, which is a well studied case of ionic–covalent curve crossing. The NACs as well as the energy gradients are $3N$-dimensional vectors in Cartesian coordinates. In Fig. 1a shows the magnitude of the NAC between the ground and the first excited states; Fig. 1b shows the difference between adiabatic energy gradients of the ground and the first excited states with respect to the internuclear distance of the two atoms as a function of the internuclear

distance. Figure 1b shows that the two gradients cross each other around 5.6 Å, where Fig. 1a shows that $N_{12}$ has a peak.

The adiabatic ($V_1$ and $V_2$) and diabatic ($U_{11}$ and $U_{22}$) potential energy curves and the diabatic coupling ($U_{12}$) are shown in Fig. 2. The two diabatic curves cross smoothly around 5.6 Å. Thus the method is successful in this simple case.

In the repulsive wall region, the energy of the adiabatic ground state increases more rapidly than the energy of the adiabatic first excited state, leading to the denominator of eqn (11) changing its sign around 1.2 Å (see Fig. 1b). At the same time the numerator is increasing as the distance between the two atoms becomes shorter (see first peak in Fig. 1a). These two features lead to a sudden state crossing at 1.2 Å with the N/D scheme, but the energy of two diabatic states are not significantly different than the adiabatic energies in this region. This results in a sudden peak in the $U_{12}$ coupling at short R, and the diabatic energies were manually switched back for the plot.

Further analysis of the LiF case is provided in the ESI.
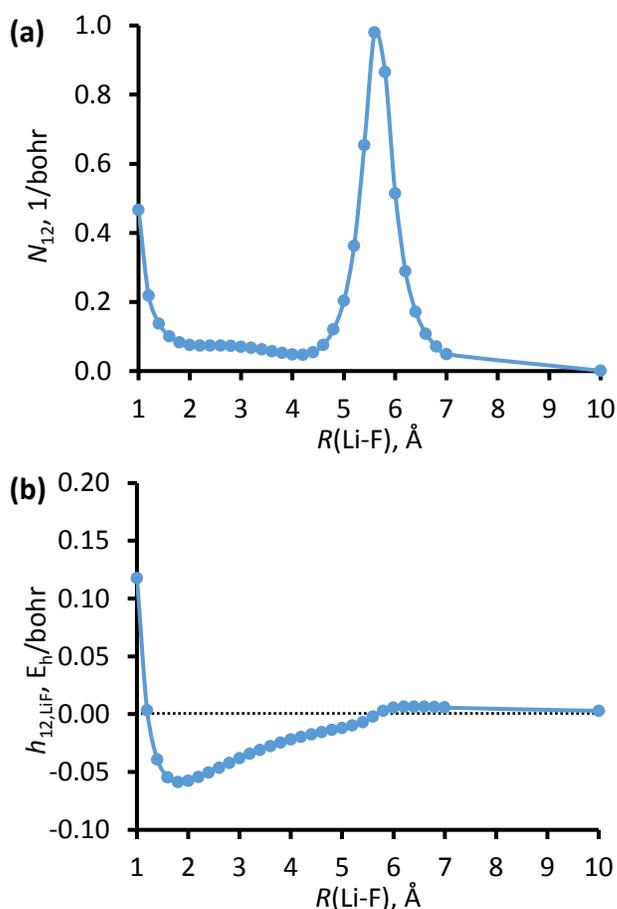


**Fig. 1** Input data for the N/D diabatization of LiF. Plot (a) shows the magnitude of the NAC between the ground and the first excited states ($N_{12}$). Plot (b) shows difference between

adiabatic energy gradients of the ground and the first excited states ($h_{12,\text{LiF}}$). The abscissa of both plots is the internuclear distance.
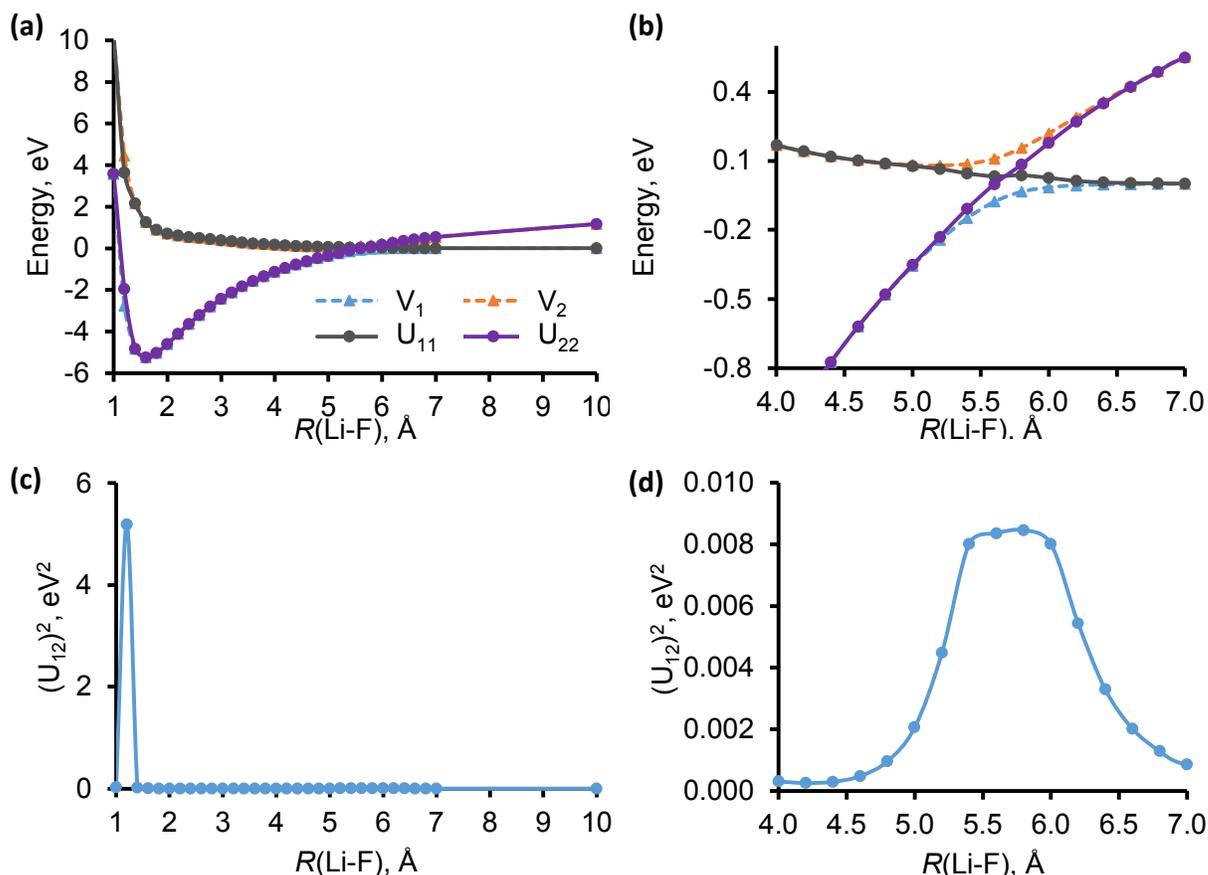


**Fig. 2** Adiabatic and diabatic potential energy curves and square of the diabatic coupling for LiF. Plot (a) shows the whole potential energy curves; plot (b) enlarges the avoided crossing region. Plot (c) show the square of the diabatic coupling, and plot (d) is another enlargement.

### 4.2. H$_3$ system

### 4.2.1. H + H$_2$ exchange reaction (H$_3$-MEP)

The minimum energy path of the H + H$_2$ exchange is collinear. The central hydrogen is labeled H$_1$ and the two terminal hydrogens are labeled H$_2$ and H$_3$. At the saddle point the two nearest-neighbor H–H bond lengths, $R_{12}$ and $R_{13}$ are equal to $R_{\text{HH}}^{\ddagger} = 1.757$ a$_0$ , and this point is defined as the origin of the reaction coordinate, which is defined as

$$s = \text{sign}\left(R_{12} - R_{\text{HH}}^{\ddagger}\right) \left(\sqrt{\left(R_{12} - R_{\text{HH}}^{\ddagger}\right)^2 + \left(R_{13} - R_{\text{HH}}^{\ddagger}\right)^2},\right. \tag{22}$$

For this example, the ground state and first excited state were taken into account. The two states are well separated in energy; the energy difference is 6.7 eV at the saddle point according to the CASSCF calculations. Thus, their crossing is widely avoided. Every component of the NAC was used to calculate the nominator $N_{12}$, which is given in Fig. 3a.

Three different diabatizations will be presented to illustrate the flexibility of the N/D method; these sets differ only the parameters used to calculate the denominator $D_{12}$. The three partial derivatives of the energy gap along the reaction path are shown in Fig. 3b. Based on the shape of these three curves, it is easy to conclude that the data set of gradient difference based on $r_{23}$ will not lead to useful diabatization as it does not cross zero (gray curve in Fig. 3b). This gradient difference was not used in eqn (20). The investigated solutions include the following sets of gradient differences. Set 1 only includes the gradient difference for $r_{12}$ (i.e, $W_{12,12} = 1$, and the other two are zero). Set 2 only includes the gradient difference for $r_{13}$ (i.e, $W_{12,13} = 1$, and the other two are zero). Set 3 includes the gradient difference from both $r_{12}$ and $r_{13}$; their weights in eqn (20) are $W_{12,12}, = 1$ and $W_{12,13} = -1$.

Both sets 1 and 2 provide smooth diabats, but the state crossing is slightly shifted away from zero (the saddle point). Set 1 shifts the crossing slightly right, and set 2 shifts the crossing slightly left. These shifts are in accord with the locations where the partial derivative differences cross zero, as shown in Fig. 3b. When the combination of the two gradient differences is used, as described in set 3, the crossing occurs at the saddle point, as expected. The solutions of diabatizations based on these three sets are shown in Fig. 4.

This illustrates an important point. When a system shows symmetry, one should take account of that symmetry when assigning the parameters. When this was done, the method is successful for the $H + H_2$ reaction. For LiF we considered a narrowly avoided crossing, and here we consider a widely avoided one; the method is successful in both cases.

**(a)**



**(b)**
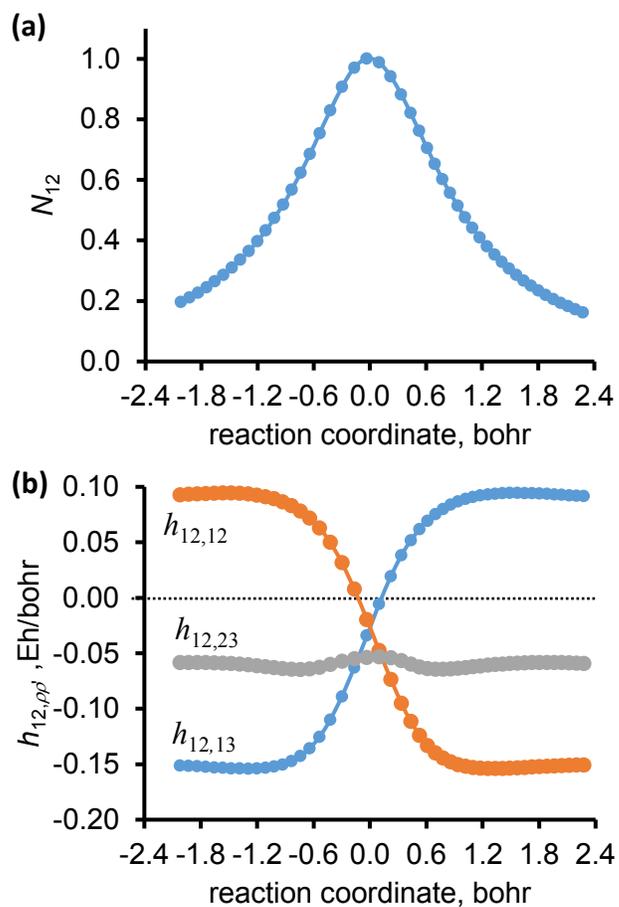


**Fig. 3** Input data for the N/D diabatization of $H_2$ + H exchange. Plot (a) shows the magnitude of the NAC between the ground and the first excited states. Plot (b) shows differences between partial derivatives (with respect to the three internuclear distances) of adiabatic energy differences I.e., gaps) of the ground and the first excited states.
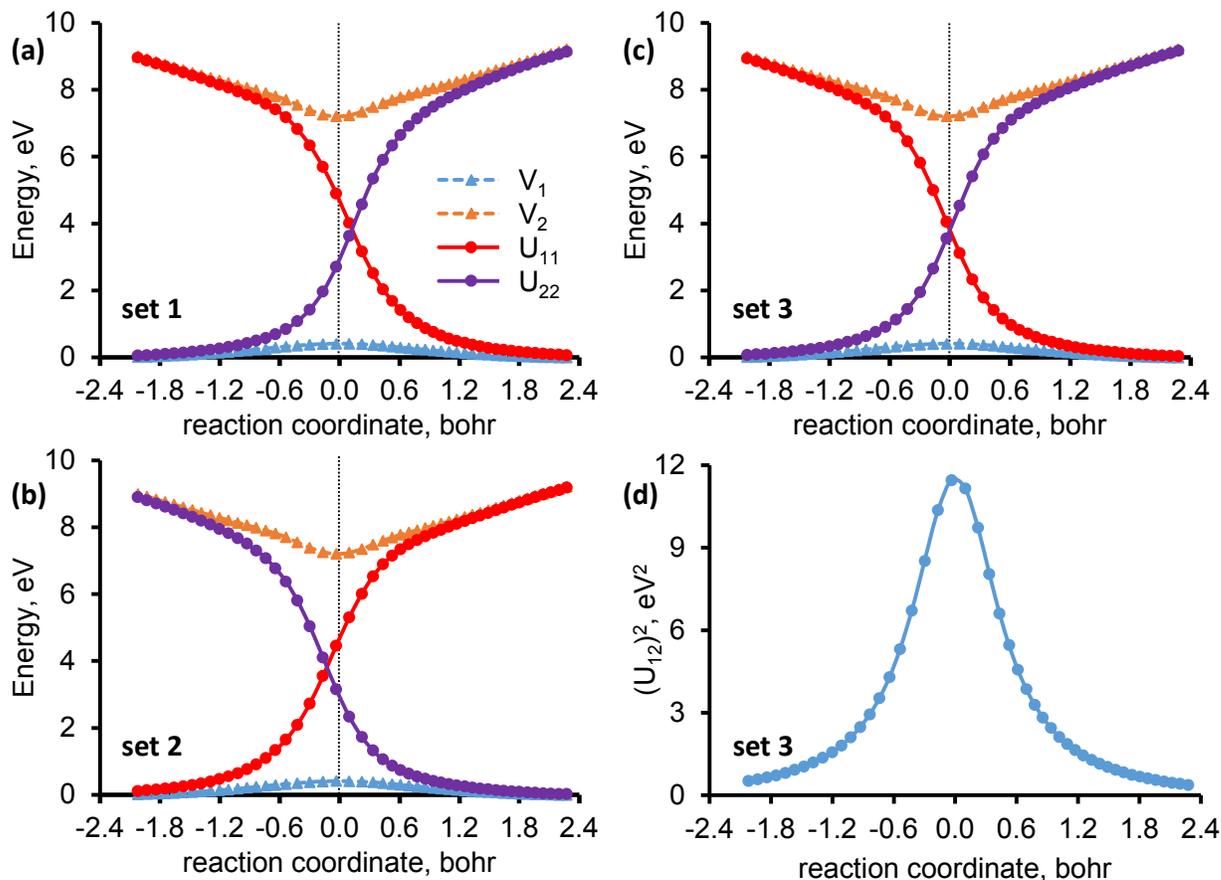
**Fig. 4** Adiabatic and diabatic potential energy curves and square of diabatic coupling for the H + $H_2$ reaction ($H_3$-MEP). Plots (a), (b), and (c) correspond to sets 1, 2, and 3, respectively. Plot (d) shows the square of the diabatic coupling in set 3.

### 4.2.3. Linear $H_3$ arrangement ($H_3$-LIN)

This example extends the consideration of the collinear $H_2$ + H reaction ($H_3$-MEP) from the minimum energy path to the full two-dimensional coordinate space. For this diabatization the $f_{thr}$ parameter is set to 0.2 $a_0^{-1}$, and the other parameters correspond to the $H_3$-MEP parameters. The results are shown in Fig. 5. The adiabatic surfaces (Fig. 5a) show an avoided crossing for geometries where $R_{12}$ and $R_{13}$ are equal. If one of the $R_{12}$ or $R_{13}$ distances is short, the adiabatic ground and the first excited states are well separated; if both $R_{12}$ and $R_{13}$ distances are long, then the system becomes three separated H atoms, and the ground and the first excited adiabatic states are degenerate.

The two diabatic surfaces, $U_{11}$ (color coded blue-to-red) and $U_{22}$ (color coded brown-to-green), smoothly cross each other at the diagonal seam (see Fig. 5b), which is a mirror plain for the collinear geometries. Away from the seam, the diabatic surfaces quickly approach the adiabatic energies where the two surfaces are not coupled. This can also be seen in the plot of the coupling squared, $(U_{12})^2$ (see Fig. 5d). When both $R_{12}$ and $R_{13}$ distances are long, the diabatic

states are degenerate. At long distances, the two adiabatic states are already degenerate, and the large NACs in this region do not affect the diabatic energies, thus their $U_{12}$ coupling remains very small.
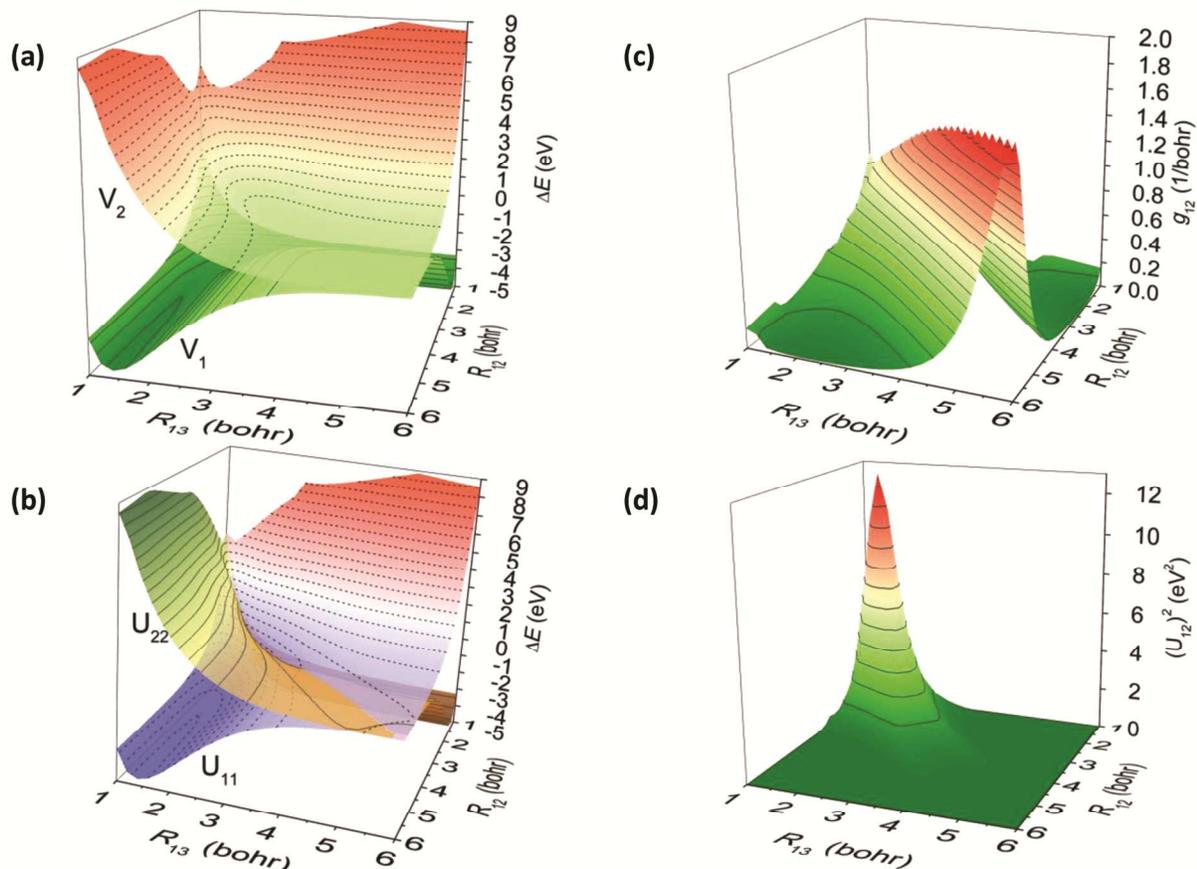


**Fig. 5** Diabatization of $H_3$-LIN data set. Plot (a) contains the two adiabatic energy surfaces, $V_1$ and $V_2$; the zero of energy is for three separated H atoms; the contour increment (solid gray lines for $V_1$ and dashed back lines for $V_2$) is 0.5 eV. Plot (b) contains the two diabatic energy surfaces, $U_{11}$ (blue-to-red) and $U_{22}$ (brown-to-green); the zero of energy corresponds to three separated H atoms; the contour increment (dashed back lines for $U_{11}$ and solid gray lines for $U_{22}$ and) is 0.5 eV. Plot (c) shows the $g_{12}$ surface, the contour increment, solid gray lines, is 0.1 bohr$^{-1}$. Plot (d) shows the surface of $U_{12}^2$, the contour increment, solid gray lines, is 1 eV$^2$.

### 4.2.3. Bent $H_3$ arrangement ($H_3$-BENT)

In this example, the $H_3$ structure is bent to 60 degrees. In this arrangement there is conical intersection seam for geometries with $R_{12} = R_{13}$. The diabatization parameters of this $H_3$-BENT system are the same as $H_3$-LIN. As expected, the $g_{12}$ values (Fig. 6c) blow up along the seam; the magnitude can go above 1 million bohr$^{-1}$ in practical calculations, and would be infinite in exact

work. The ground and the first excited adiabatic states become degenerate along the seam, which is the diagonal of the plot (see Fig. 6a). The two diabatic surfaces, $U_{11}$ (blue-to-red) and $U_{22}$ (brown-to-green), smoothly cross each other along the diagonal of the plot (see Fig. 6b). On the two sides of the seam, the diabatic surfaces approach the adiabatic surfaces as the two surfaces are not strongly coupled. This can also be seen in plot of coupling squared, $(U_{12})^2$ where the coupling decreases away from the seam (see Fig. 6d). The diabatic coupling increases as it approaches the seam, but right at the seam the two adiabatic states are degenerate, as are the diabatic states, and the $U_{12}$ coupling is zero.
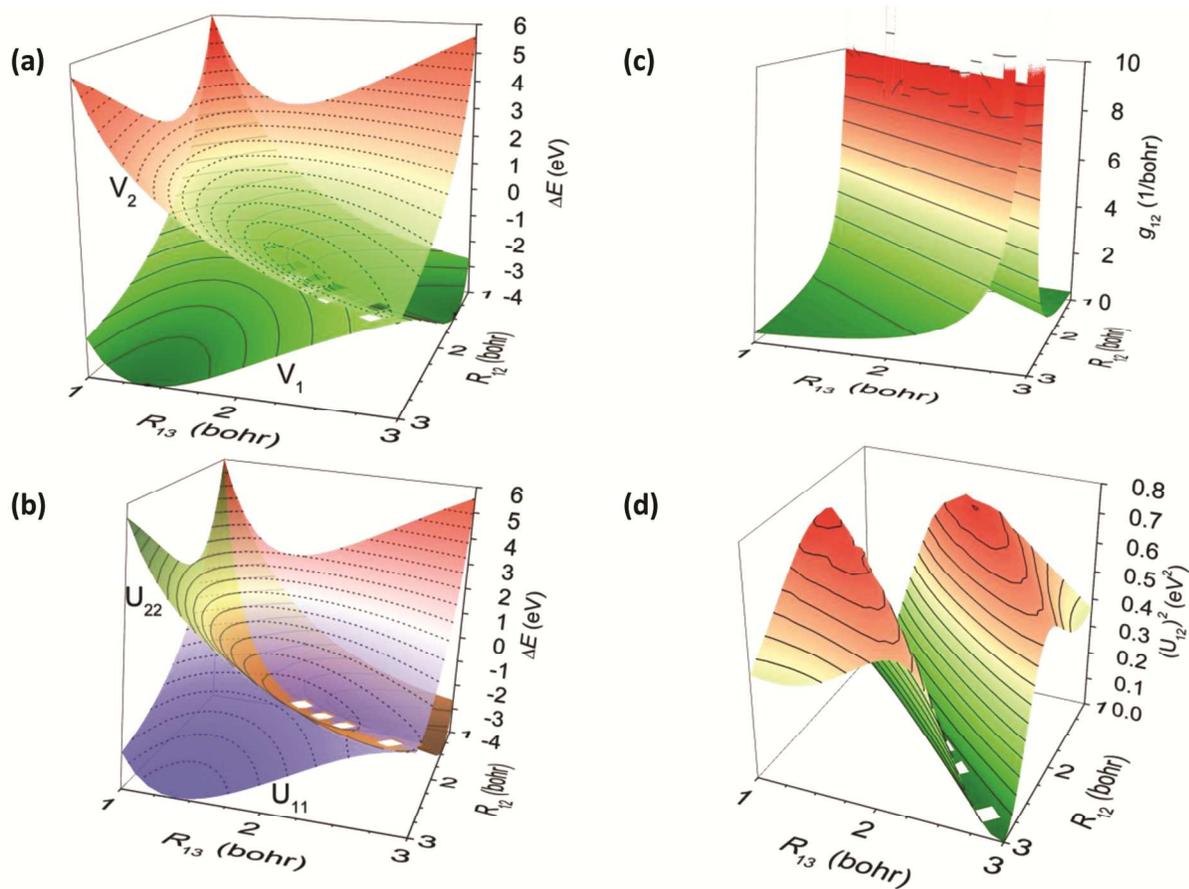


**Fig. 6** Diabatization of $H_3$-BENT data set. Plot (a) contains the two adiabatic energy surfaces, $V_1$ and $V_2$; the zero of energy is the three separated H atoms; the contour increment (solid gray lines for $V_1$ and dashed back lines for $V_2$) is 0.5 eV. Plot (b) contains the two diabatic energy surfaces, $U_{11}$ (blue-to-red) and $U_{22}$ (brown-to-green); the zero of energy is again for three separated H atoms; the contour increment (dashed back lines for $U_{11}$ and solid gray lines for $U_{22}$ and) is 0.5 eV. Plot (c) shows a part of $g_{12}$ surface (at the conical intersection seam $g_{12}$ can go above 1 million bohr$^{-1}$) the contour increment, solid gray lines, is 1 bohr$^{-1}$. Plot (d) shows the surface of $(U_{12})^2$, the contour increment, solid gray lines, is 0.05 eV$^2$. Note that we were not able to

calculate four points along this seam; those geometry points are left out and they appear as empty regions of the plots.

### 4.3 $H_2$ dimer

The $H_2$ dimer was previously calculated by both the fourfold way and DQΦ (in particular by the Boys localized, DQ, and DΦ special cases of DQΦ).[9,15] The four atoms are collinear, and we consider a system consisting of two hydrogen molecules with centers of mass separated by 10 $a_0$ and with each molecules starting with a bond distance of $R_0 = 1.5$ $a_0$. The bond lengths of the two molecules are simultaneously changed by $\Delta R$; one of the $H_2$ bond distances is decreased ($R_0 - \Delta R$) and the other $H_2$ bond distance is increased ($R_0 + \Delta R$). The range of $\Delta R$ is -0.2 to 0.2 $a_0$. This reaction coordinate results in one bond switching from stretched to compressed while the other molecule simultaneously goes from compressed to stretch. When $\Delta R$ is zero, the two bond lengths are equal (at the middle of the reaction coordinate). Along this reaction path, the first and second excited states (i.e., states 2 and 3, both $^1\Sigma^+$), show a locally avoided crossing in the adiabatic representation. These two crossing states are energetically well separated from the ground state.

To carry out the N/D diabatization, we considered two possible ways to proceed. The ground state is well separated from the other two states and the ground state is only slightly coupled with either of the two excited states; see Fig. 7a. Therefore, in the first set of calculations, a simple two-by-two diabatization is carried out for state pair $ij = 23$. The partial derivatives of the 2-3 energy gap are shown in Fig. 7d for the six possible internuclear distances. We label the atoms left to right: 1,2 for the first $H_2$ and 3,4 for the second $H_2$. As can be seen in the plot, four of the curves can lead to useful diabatization, but, similarly to the situation in subsection 4.2, the diabats based on a single atom pair set would suffer from some asymmetry. Therefore, we again take a linear combination to get symmetric diabatic energy curves. Among the possible combinations, we only show the one for which the weights $W_{23,\rho\rho'}$ are 1.0, 1.0, -1.0, 1.0, -1.0, and -1.0 with respect to internuclear ditances, $R_{12}$, $R_{13}$, $R_{14}$, $R_{23}$, $R_{24}$, and $R_{34}$, respectively. The two diabatic curves cross smoothly where the two $H_2$ molecules have equal bond lengths ($R_{12} = R_{34}$) as shown in Fig. 8.

A second set of calculations is shown for a three-by-three diabatization. The differences of the partial energy derivatives with respect to the six possible internuclear distances for state pairs 12 and 13 are shown in Figs. 7b and 7c. For all three $jk$ state pairs, the weights $W_{jk,\rho\rho'}$ were selected to be 1.0, 1.0, 0.0, 0.0, -1.0, and -1.0 for the partial derivatives with respect to the six internuclear distances in the same order as above. Figure 9 shows the result of this diabatization. In this diabatization the couplings of state pairs 12 and 13 are stronger than that of state pair 23, but state 1 is well separated from the other two states in energy, thus those couplings do not

cause the diabatic energy curves to differ noticeably from the adiabatic ones in Fig. 9a. As expected, diabatic states 2 and 3 cross each other where the two $H_2$ molecules have equal bond lengths. Thus both strategies yield useful diabats, but the simpler two-state treatment r probably preferable.

If one used larger $W_{12,\rho\rho'}$ and $W_{13,\rho\rho'}$, the couplings of state pairs 12 and 13 would be further decreased, but for all examples shown in the present article, $W_{jk,\rho\rho'}$ is independent of $j$ and $k$.
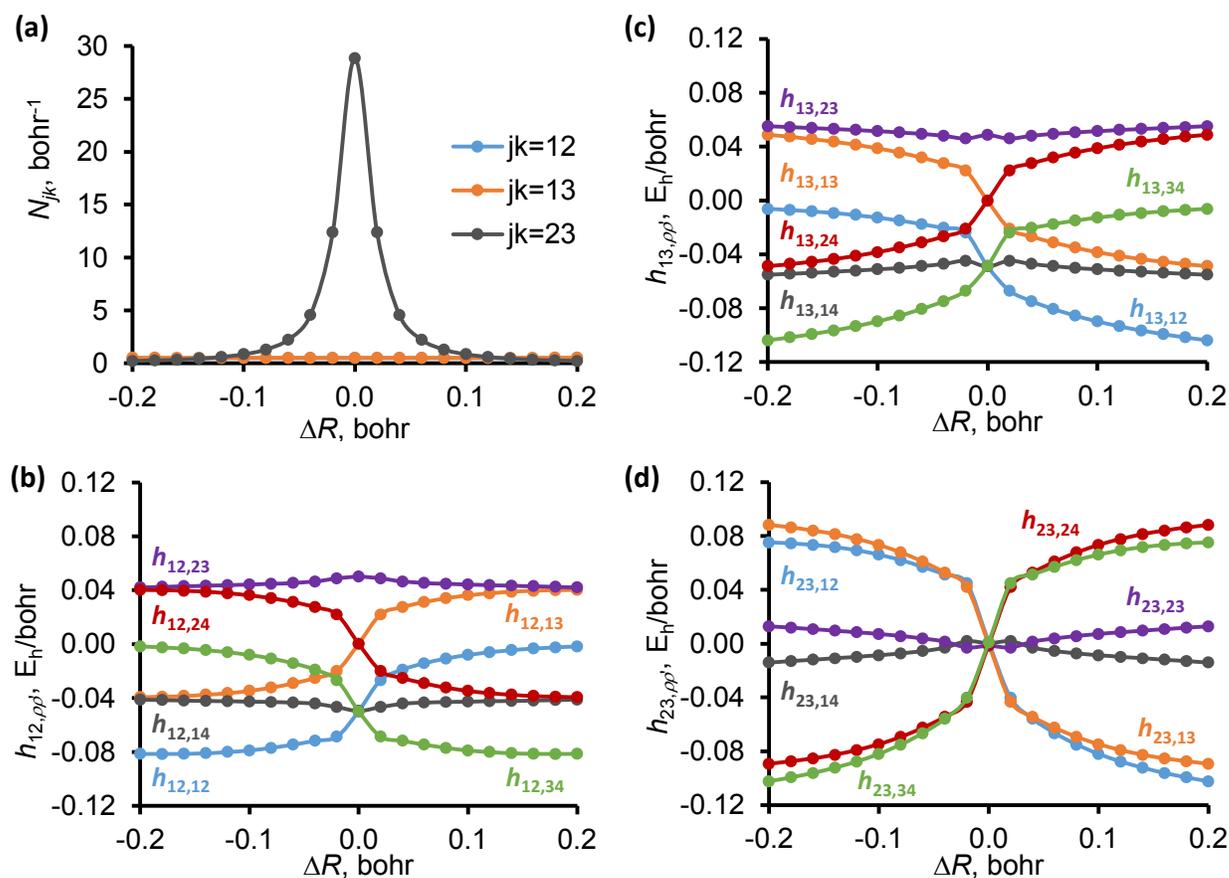


**Fig. 7** Input data for the N/D diabatization of $H_2$ dimer. Plot (a) shows the magnitudes of the NACs between state pairs 12, 13, and 23. Plots (b), (c), and (d) show differences between adiabatic energy gradients of state pairs 12, 13, and 23, respectively, with respect to the six internuclear distances.
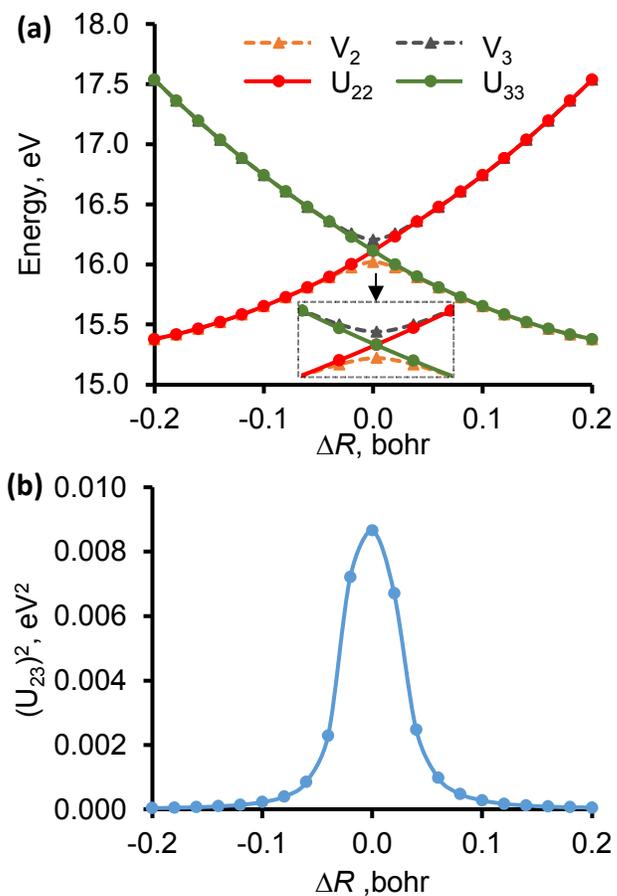
**Fig. 8** Adiabatic and diabatic potential energy curves (part a) and the square of the diabatic coupling (part b) for $H_2$ dimer based on a two-by-two diabatization for state pair 23 ("set 1" diabatization).
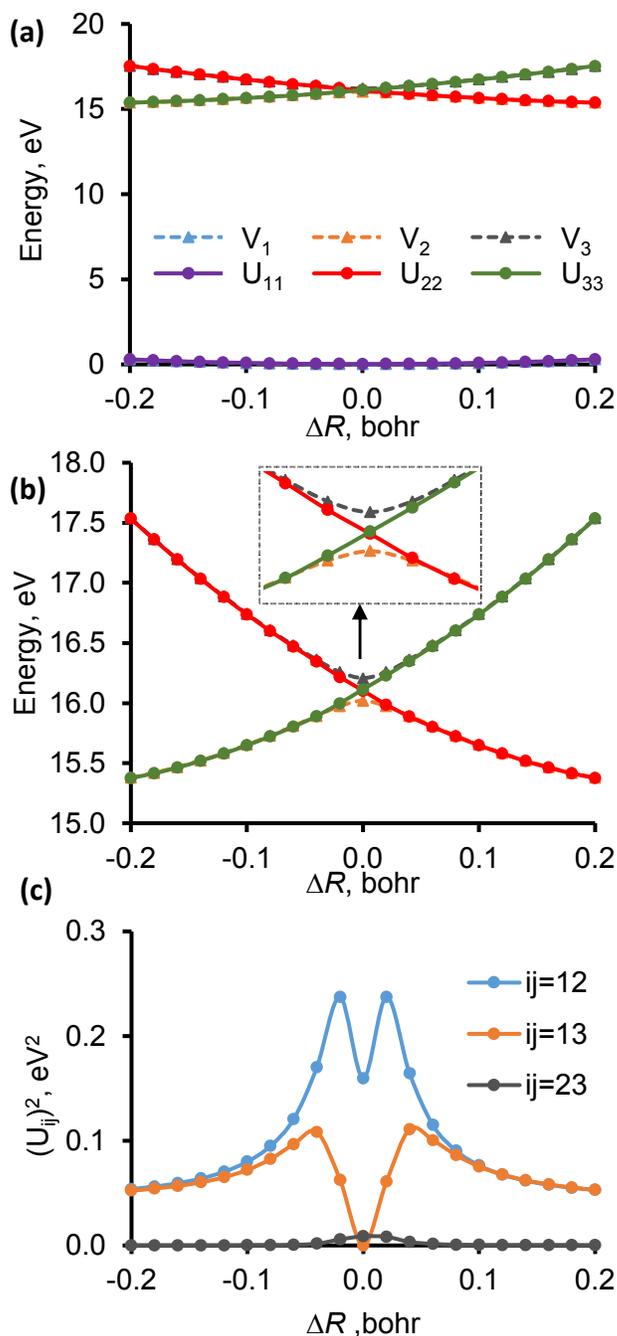
**Fig. 9** Adiabatic and diabatic potential energy curves (a) as well as their coupling (c) of $H_2$ dimer based on a three-by-three diabatization ("set 2" diabatization). Plot (b) enlarges the coupling region of state pair 23.

## 4.4. LiHF

The LiFH system involves the reaction: $Li(^2S, ^2P) + FH \rightarrow LiF + H$. The ground and first excited states in the reactant region, $1\,^2A'$ and $2\,^2A'$, correspond to the Li atom in the $^2S$ and $^2P$

states, respectively. In the products region, the ground state has a singly occupied H($1s$) orbital and the first excited state corresponds to electron donation from an in-plane lone pair on the F to the H atom, which becomes very high in energy along the product coordinate. The reaction coordinate has been previously defined in a fourfold way and DQΦ study.[9,15] The zero of the coordinate is located at the saddle point of the lower adiabatic potential curve. The positive side of the coordinate corresponds to motion towards LiF + H, the products; the negative side corresponds to motion towards LiH + F, the reactants. Distances between successive points along the reaction coordinate are defined by

$$\Delta s = \sqrt{\Sigma_{\rho=\mathrm{Li,F,H}}\left(\Delta X_\rho^2 + \Delta Y_\rho^2 + \Delta Z_\rho^2\right)} \tag{23}$$

where $\Delta X_\rho, \Delta Y_\rho,$ and $\Delta Z_\rho$ corespond to differences in mass-weighted Cartesian coordinates of the atoms (this definition only affects the scale of the abscissa in plots; it has no effect on diabatization).

Previous calculations with the fourfold way and DQΦ diabatization method were successful.[9,15] However, the fourfold way required a reference orbital, and the introduction has already pointed out that it would be desirable to avoid reference orbitals, because defining them may require an in-depth knowledge of the system. Three partial derivative differences for this two-state problem are shown in Fig. 10b. These partial derivatives correspond to the LiF, LiH, and FH internuclear distances. Among these three curves, the FH data set, labeled set 1, ($W_{12,\mathrm{FH}} = 1, W_{12,\mathrm{LiF}} = 0,$ and $W_{12,\mathrm{FH}} = 0$) and the LiF data set, labeled set 2, ($W_{12,\mathrm{LiF}} = 1$ and the other two weights are zero) can lead to useful diabatization, since these curves change sign near the saddle point. The two predicted diabatic energy sets are slightly different; when using set 1, the crossing is shifted towards the reactant side as compared to set 2, see Fig. 11a and 11b. We also investigated a linear combination of the three partial derivatives (set 3), where the $W_{12,\rho\rho'}$ weights in eqn (20) are 1.0, 1.0, and -1.0 for the LiF, LiH, and FH partial derivatives, respectively. For all three sets, $g_{12}$ (which appears in the nominator) is shown in Fig. 10a. Figures 11a, 11b, and 11c show very good agreement between the three sets of diabatization. As diabats are not unique, all three solutions to the diabatization problem can be acceptable, and one could choose which set of diabats to use based on other considerations, for example, on the behavior in other regions of geometry.
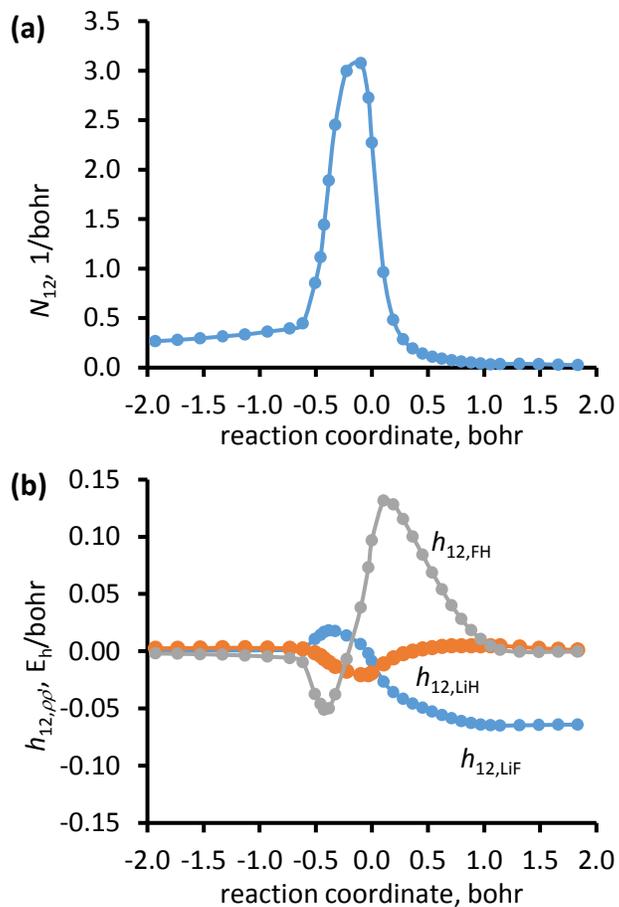
**Fig. 10** Input data for the N/D diabatization of reaction Li($^2$S, $^2$P) + FH → LiF + H. Plot (a) shows the magnitude of the NACs between the ground and the first excited states. Plot (b) shows differences between adiabatic energy gradients of the ground and the first excited states ($h_{12,\rho\rho'}$) with respect to the three internuclear distances.
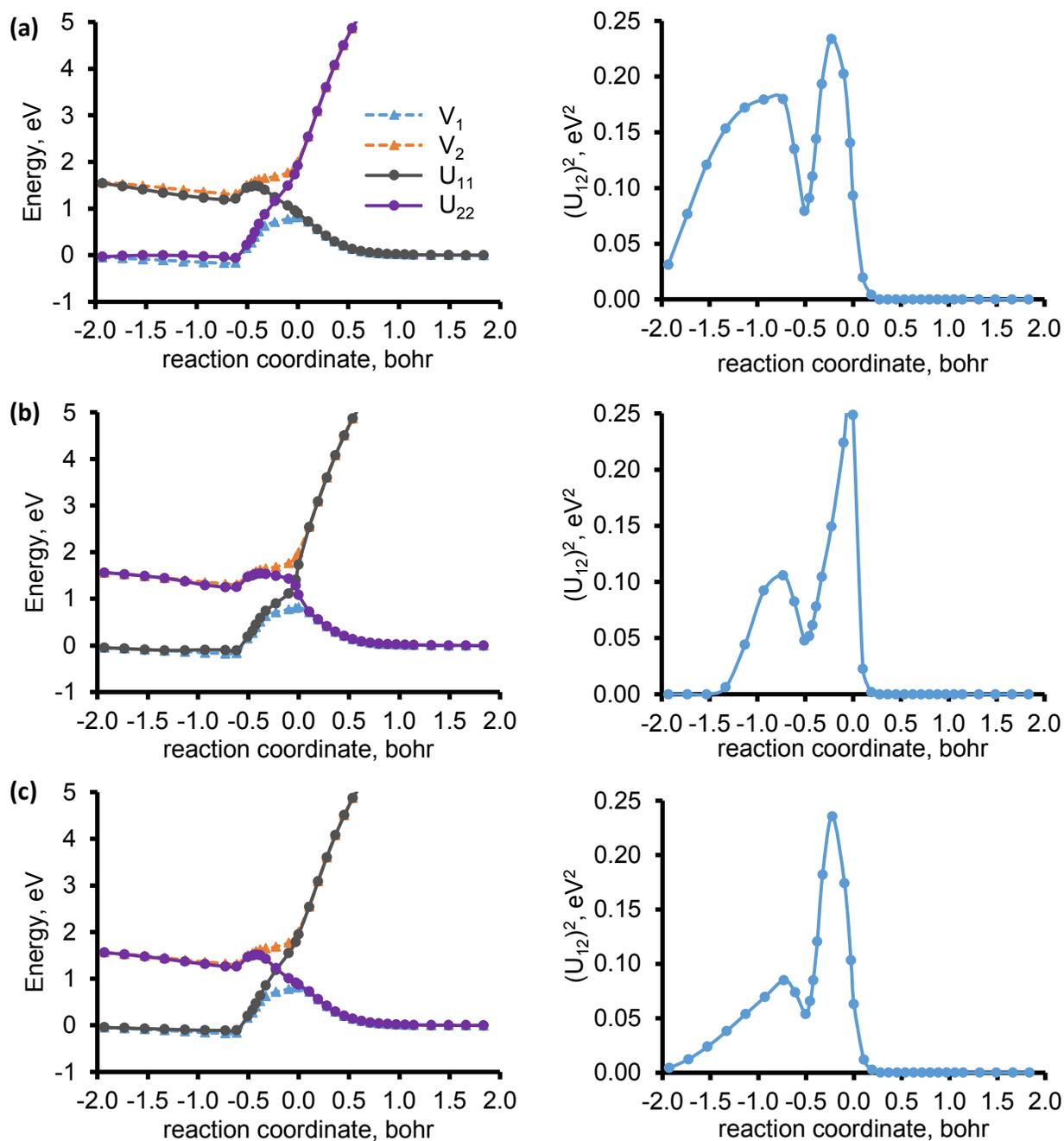
**Fig. 11** Adiabatic and diabatic potential energy curves (right plots) as well as their coupling (left plots) of Li($^2$S, $^2$P) + FH $\rightarrow$ LiF + H. The plots on the right show the square of the coupling element of state pair 12. Plots (a), (b), and (c) correspond to sets 1, 2, and 3, respectively.

## 4.5. Phenol

The photodissociation of phenol has previously been modeled as a three-state process;[70] as the O-H bond dissociates, the system passes two conical intersections.[12] The electronic configuration of the ground adiabatic state at dissociation corresponds to the configuration of the

third adiabatic state at the equilibrium bond distance of OH. The minimum energy pathway of the dissociation occurs in a planar structure, and the presence of conical intersections is clearly seen in the shapes of the adiabatic potential energy curves. To show our results for a nonsymmetrical path, we distorted the geometry by turning the dissociating hydrogen out of the plane of the phenoxyl radical by the torsion angle $\theta$, where $\theta = 45°$. Along the O–H bond dissociation path at this fixed torsion angle, the presence of one of the state crossings is no longer in the shapes of the adiabatic energy curves, so this provides a good test.

Phenol is a larger system than our previous examples, and it is used to illustrate that NAC components for atoms far from the reaction center are not essential for diabatization. The NAC components are typically nonzero even when we expect the diabats to be very similar the adiabats, and as we include more NAC components these nonzero components add up. However, most of those components could be considered to be "background noise", and, if included, that noise could obscure the useful NAC components that carry the physics of the state crossing. As an example, in Fig. 12 we compare the whole magnitude of NAC components of all atoms (plot 10a) with only the magnitude of NAC components of the oxygen atom and the dissociating hydrogen atom (plot 10b). In both plots, the NAC elements predict a sharp state crossing around 1.3 Å for states 2 and 3, and a wide state crossing around 1.9 Å for states 1 and 2. However, as we move away from the crossings, the curves in plot 10b approach zero along the OH dissociation, but in plot 10a we still see significant NAC values at large values of the dissociation coordinate. Therefore we carried out N/D diabatization by using in the numerator only the NAC components shown in Fig. 12b.

The partial derivative differences used in the denominator for state pairs 1 and 2, 1 and 3, and 2 and 3 are shown in Fig. 12c as functions of the OH distance.

Figure 13 shows the adiabatic potential energy curves and the diabatic potential energy curves and squares of the diabatic couplings obtained by the N/D method. Both of the avoided state crossings in the adiabatic representations have smooth state crossings in the diabatic representation. One can see a significant coupling for $U_{13}$ at 1.3 Å. At this geometry, the diabatic energy difference of the two coupled states is large ($\sim$ 4.2 eV), thus this coupling barely affects the shapes of the potential curves.
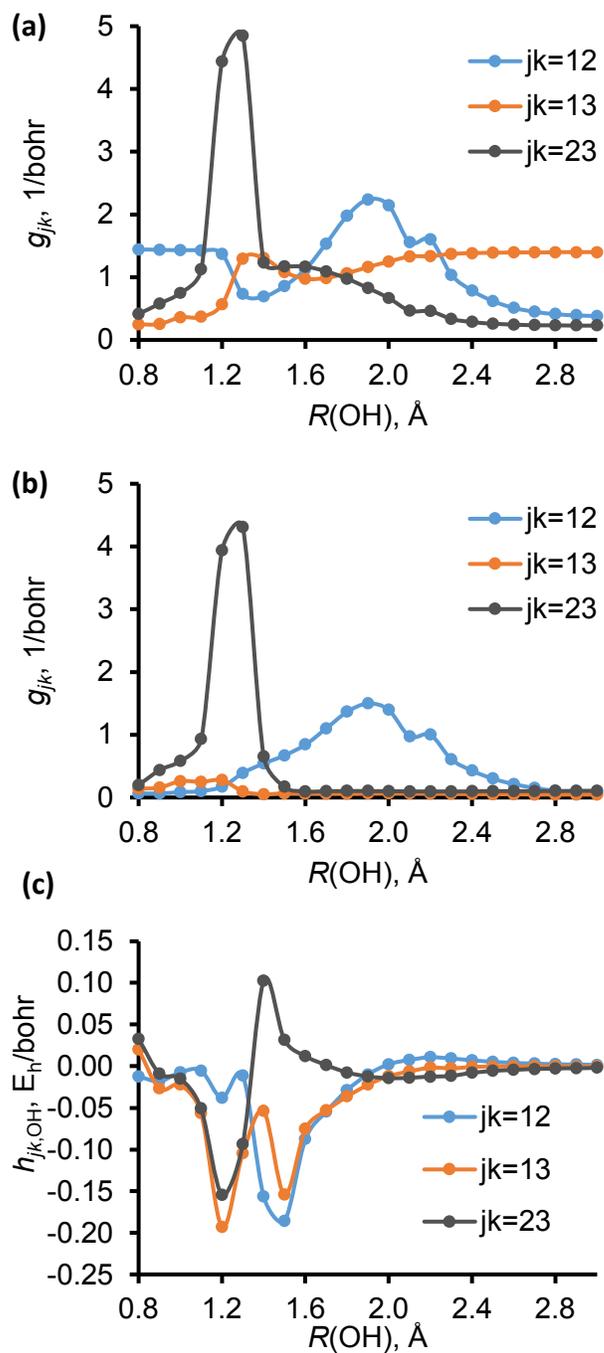
**Fig. 12** Plot (a) shows the magnitude of all NAC components for state pairs 12, 13, and 23. Plot (b) shows the magnitude of the NAC components of oxygen and the dissociating hydrogen for state pairs 12, 13, and 23. Plot (c) shows the differences between adiabatic energy gradients of state pairs 12, 13, and 23 with respect to the (dissociating) OH internuclear distance.
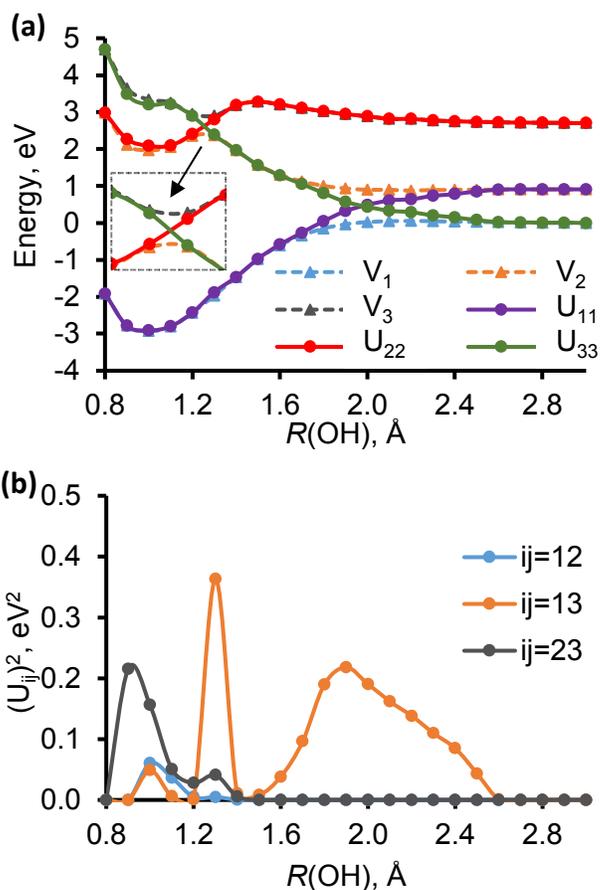
**Fig. 13** Adiabatic and diabatic potential energy curves (a) as well as their coupling (b) of phenol dissociation ($\theta = 45°$).

### 4.6. $O_3$ system

The $O_3$ system was previously treated with DQΦ.[15] In that paper, two cuts of the first two $^1A''$ singlet states along the asymmetrical ozone stretch were shown where the three oxygen atoms were fixed at 120 and 100 degrees, and one of the bond lengths was also fixed. The other bond length was varied to show the avoided crossing of the first two $^1A''$ singlet states along the asymmetrical ozone stretch. In that article, the NAC curves along the bond stretch were presented (see Figs 19 and 22 in Ref. 15) and they clearly show the coupling between the two states of interest. Here we apply the N/D method to this problem.

In the new calculations, the first three $^3A'$ states were calculated. The bond angle of the three oxygen atoms was fixed at 175 degrees, i.e., the atoms are almost collinear. One of the bond lengths was fixed at the equilibrium distance of $O_2$ molecule, $R_e = 1.208$ Å. The other bond length was varied between 1 and 3 Å. At large $O_2(\,^3\Sigma_g^-) + O(^3P)$ distances, the first two $^3A'$ states correspond to the threefold degenerate ground state of $O(^3P)$ atom (the third component of the ground state is the first $^3A''$ state). The first excited asymptote corresponds to the $O_2(\,^1\Delta_g) + O(^3P)$ combination. This asymptote has six-fold spatial degeneracy, with three $^3A'$ and three $^3A''$

states. The second excited $^3A'$ state is one of these six states in the $^3A'$ representation. For a complete treatment, one should include all low-energy states, but the three states considered here are enough to enough to compare DQΦ to the new N/D method.

Figure 14 shows that as the distance between the molecule and the atom is decreased, the adiabatic energy of the first excited state (orange dashed curve) increases more rapidly than the adiabatic energy of the ground state (blue dashed curve). Around 1.8 Å, there is a locally avoided crossing for the first and the second (gray dashed curve) adiabatic excited states. Both the first and the second adiabatic excited-state potentials show breaks at 1.3 Å. This is a clear sign of further avoided crossing with higher energy states not present in this plot.

Figure 14a shows a diabatization solution based on DQΦ method (in the notation of the DQΦ method,[15] the parameters are $\gamma = 1.0$ a.u. for the dipole, $\alpha = 1.0$ a.u. and origin at center of mass for the quadrupole, and $\beta = 1.0$ a.u. for the electrostatic potential at the center of mass). Many other combinations of $\alpha$, $\beta$, $\gamma$, and origins were tried, but none of them could qualitatively improve the diabatization scheme. As it can be seen, the predicted diabatic energy curves (purple, red, and green) become degenerate, i.e., the DQΦ method is not successful.

The N/D diabats are much better; they smoothly cross, as shown in Fig. 14b. For this diabatization the magnitude of the all NAC components was used; see Fig. 15a. According to the NACs, we expect three state crossings along the $O_2 + O$ reaction path. Starting from longer distance, there is a coupling for states two and three ($g_{23}$) at 1.8 Å. Then the ground and the first excited states should cross ($g_{12}$) around 1.6 Å. Finally, states two and three ($g_{23}$) have to cross, again, at 1.4 Å. We label the central O as atom 1; in the denominator the gradient difference from both $r_{12}$ and $r_{13}$ were used with 1.0 and -1.0 weights

Again the N/D method provides acceptable and useful results.
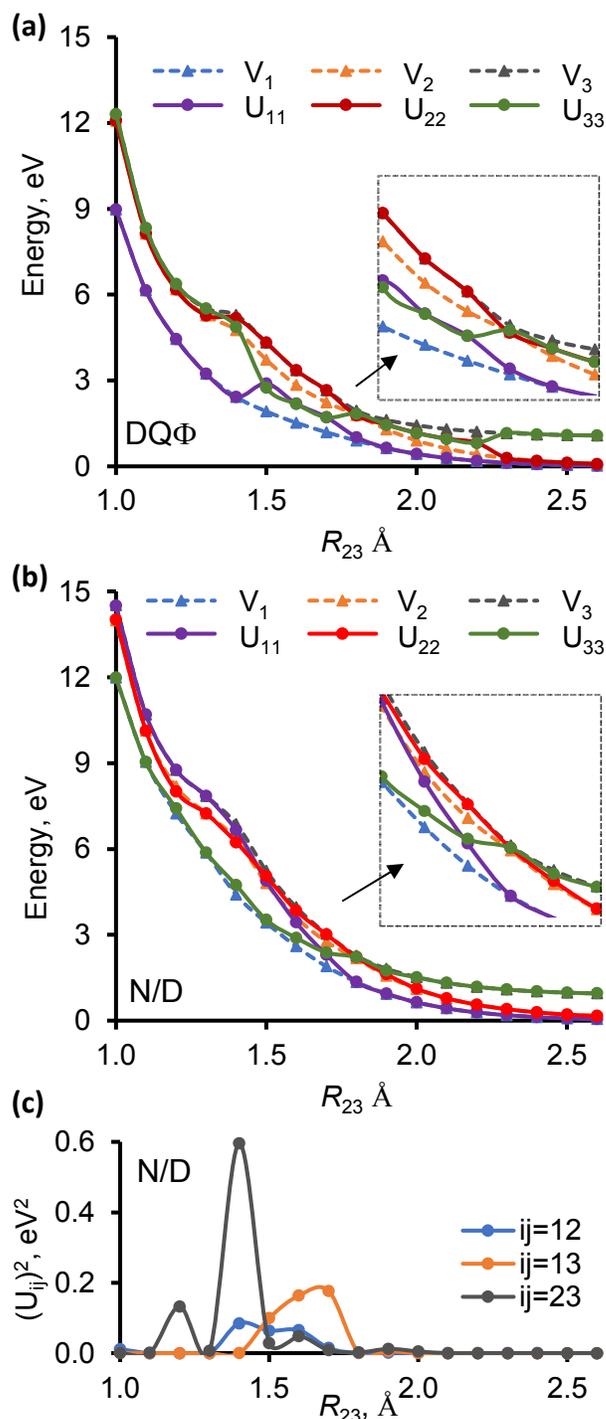
**Fig. 14** Adiabatic and diabatic potential energy curves of an $^3A'$ $O_2(^3\Sigma_g^-)$ + O($^3$P) collision, for details see the text. Plot (a) shows a flawed diabatization by DQΦ method. Plot (b) shows a diabatization by N/D method, and the diabatic coupling of N/D are shown in plot (c). For part a, the adiabatic energies and one-electron properties were calculated by XMS(3)-CASPT2; for parts b and c, the results are based on SA(3)-CASSCF; this difference does not introduce qualitative differences.
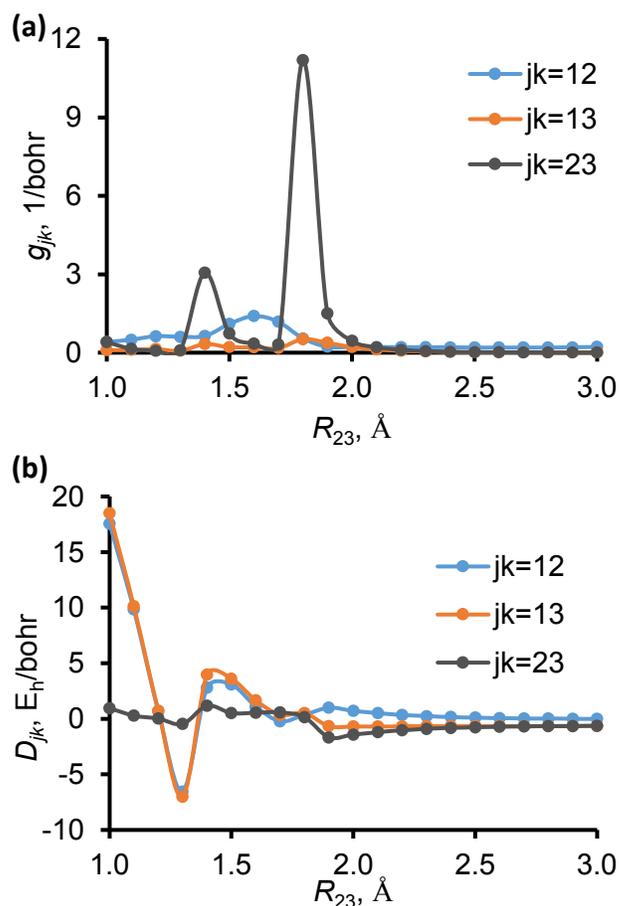
**Fig. 15** Plot (a) shows the magnitude of all NAC components for state pairs 12, 13, and 23. Plot (b) shows the selected denominators in eqn (20) for state pairs 12, 13, and 23, for details see the text.

## 5. Concluding remarks

Diabatic states can provide relevant chemical insight into an electronically adiabatic system by uncovering the smooth electronic configurations that underlie the adiabatic states. In principle, one could use only the nonadiabatic couplings to carry out diabatization; however, we show here that incorporation of the adiabatic energy gradients into the procedure makes the diabatization process very convenient because the difference of the energy gradients carries useful information about the underlying diabatic states. The article shows how the nonadiabatic couplings and the gradients of the adiabatic states, when used together, provide a very convenient way to uncover the underlying diabatic states. In addition to providing chemical insight, diabatization is very useful for enabling fitting of potential energy surfaces and couplings so one may carry our efficient simulations of dynamics.

Thus we present a new diabatization method based on NACs and differences of energy gradients, and it is called the N/D method. The N/D method is a direct, orbital-independent diabatization scheme. It is adiabatic-equivalent and can therefore be converted back to an adiabatic representation by diagonalizing the diabatic Hamiltonian matrix. One can then use the adiabatic or diabatic representation to carry out dynamics simulations and study reaction rate constants, energy transfer rate constants, and photochemical mechanisms.

We showed that the N/D method can be successfully applied to systems previously analyzed with the fourfold way and the DQ$\Phi$ method including LiF, $(H_2)_2$, Li + HF, and phenol. We also provide successful applications to the $H_3$ system and $O + O_2$ interactions. The N/D method avoids working with orbitals, which makes the N/D scheme easier to use than the fourfold way. We applied the DQ$\Phi$ and N/D methods to the three $^3A'$ triplet states of $O_3$ and showed that while the DQ$\Phi$ method failed to give smooth, reasonable diabats, the N/D method was successful; the three adiabatic properties included in the DQ$\Phi$ method failed to distinguish diabatic states, but the N/D method included sufficient information about the adiabatic states to discover underlying diabats.

The N/D method requires some system-dependent decisions, but this is a common requirement for diabatization methods or indeed for many methods of calculating adiabatic electronic states. For the N/D method these decisions include choosing the nonadiabatic coupling vector components and adiabatic gradient components and weights as well as thresholds and scaling factors. Although further analysis might lead to systematic ways to choose these parameters, in all six cases considered here we were able to find suitable values of the parameters.

## Conflicts of interest

There are no conflicts to declare.

## Acknowledgements

# References

[1] A. W. Jasper, B. K. Kendrick, C. A. Mead and D. G. Truhlar, "Non-Born-Oppenheimer Chemistry: Potential Surfaces, Couplings, and Dynamics," in *Modern Trends in Chemical Reaction Dynamics: Experiment and Theory (Part 1)*, edited by X. Yang and K. Liu (World Scientific, Singapore, 2004), pp. 329-391.

[2] C. A. Mead and D. G. Truhlar, *J. Chem. Phys.*, 1982, **77**, 6090.

[3] W. Lichten, *Phys. Rev.*, 1967, **164**,131.

[4] F. T. Smith, *Phys. Rev.,* 1969, **179**, 111.

[5] T. F. O'Malley, *Adv. At. Mol. Phys.*, 1971, **7**, 223.

[6] H.-J. Werner and W. Meyer, *J. Chem. Phys.*, 1981, **74**, 5802.

[7] K. Ruedenberg and G. J. Atchity, *J. Chem. Phys*., 1993, **99**, 3799

[8] G. J. Atchity and K. Ruedenberg, *Theor. Chem. Acc.*, 1997, **97**, 47.

[9] H. Nakamura and D. G. Truhlar, *J. Chem. Phys.*, 2001, **115**, 10353.

[10] H. Nakamura and D. G. Truhlar, *J. Chem. Phys.*, 2002, **117**, 5576.

11 H. Nakamura and D. G. Truhlar, J. Chem. Phys., 2003, 118, 6816.

[12] X. Xu, K. R. Yang and D. G. Truhlar, *J. Chem. Theory Comput.*, 2013, **9**, 3612.

[13] J. E. Subotnik, S. Yeganeh, R. J. Cave and M. A. Ratner, *J. Chem. Phys.*, 2008, **129**, 244101.

[14] E. Hoyer, X. Xu, D. Ma, L. Gagliardi and D. G. Truhlar, *J. Chem. Phys*., 2014, **141**, 114104.

[15] E. Hoyer, K. Parker, L. Gagliardi and D. G. Truhlar, *J. Chem. Phys*., 2016, **144**, 194101.

[16] R. Thürwachter and P. Halvick, *Chem. Phys.*, 1997, **221**, 31.

[17] W. Domcke and C. Woywood, *Chem. Phys. Lett*., 1993, **216**, 362.

[18] D. Simah, B. Hartke and H.-J. Werner, *J. Chem. Phys*., 1999, **111**, 4523.

[19] D. G. Truhlar, *J. Comput. Chem.*, 2006, **28**, 73.

[20] L. Song and J. Gao, *J. Phys. Chem. A*, 2008, **112**, 12925.

[21] C. A. Mead and D. G. Truhlar, *J. Chem. Phys.*, 1979, **70**, 2284.

[22] M. S. Child, "Electronic Excitation: Nonadiabatic Transitions," in *Atom-Molecule Collision Theory*, edited by R. B. Bernstein (Plenum, New York, 1979), pp. 427-465.

[23] G. A. Meek and B. G. Levine, *J. Chem. Phys.*, 2016, **144**, 184109.

[24] W. H. Press, B. P. Flannery, S. A. Teukolsky and W. T. Vetterling "Jacobi Transformation of a Symmetric Matrix." 11.1 in Numerical Recipes in FORTRAN: The Art of Scientific Computing, 2nd ed. Cambridge, England: Cambridge University Press, pp. 456-462, 1992.

[25] D. R. Bates and R. McCarroll, *Proc. R. Soc. London Ser. A*, 1958, **245**, 175.

[26] W. R. Thorson, *J. Chem. Phys.*, 1965, **42**, 3878.

[27] C. F. Melius and W. A. Goddard III, *Chem. Phys. Lett.*, 1972, **15**, 524.

[28] J. C. Y. Chen, V. H. Ponce and K. M. Watson, *J. Phys. B*, 1973, **6**, 965.

[29] W. R. Thorson and J. B. Delos, *Phys. Rev. A*, 1978, **18**, 117.

[30] Y. Hahn, *J. Phys. B*, 1978, **11**, 3221.

[31] B. C. Garrett and D. G. Truhlar, "The Coupling of Electronically Adiabatic States in Atomic and Molecular Collisions," in *Theoretical Chemistry: Advances and Perspectives*, Vol. 6A, edited by D. Henderson (Academic Press, New York, 1981), pp. 215-289.

[32] J. B. Delos, *Rev. Mod. Phys.*, 1981, **53**, 287.

[33] B. C. Garrett, D. G. Truhlar and C. F. Melius, "Derivative Coupling Elements in Electronically Adiabatic Representations and Their Use in Scattering Calculations," in *Energy Storage and Redistribution in* Molecules, edited by J. Hinze (Plenum Press, New York, 1983), pp. 375-395.

[34] M. Kimura, S. Chapman and N. F. Lane, *Phys. Rev. A*, 1986, **33**, 1619.

[35] A. Macias, *J. Phys. B*, 1987, **20**, 295.

[36] L. F. Errea, C. Harel, H. Jouin, L. Méndez, B. Pons and A. Riera, *J. Phys. B*, 1994, **27**, 3603.

[37] G. Hose, *Phys. Rev. A*, 1995, **51**, 2199.

[38] R. J. Buenker and Y. Li, *J. Chem. Phys.*, 2000, **112**, 8318.

[39] A. K. Belyaev, A. Dalgarno, and R. McCarroll, *J. Chem. Phys.*, 2002, **116**, 5395.

[40] Varandas, A. J. C. *J. Chem. Phys.*, 2009, **131**, 124128.

[41] A. K. Belyaev, *Phys. Scripta*, 2009, **80**, 048113.

[42] A. K. Belyaev, *Phys. Rev. A*, 2010, **82**, 060701.

[43] S. Fatehi , E. Alguire, Y. Shao , and J. E. Subotnik, *J. Chem. Phys.*, 2011, **135**, 234105.

[44] Q. Ou, S. Fatehi , E. Alguire, Y. Shao , and J. E. Subotnik, *J. Chem. Phys.*, 2014, **141**, 024114.

[45] B. K. Kendrick, C. A. Mead, and D. G. Truhlar, *Chem. Phys.*, 2002, **277**, 31.

[46] H.-J. Werner, P. J. Knowles, G. Knizia, F. R. Manby and M. Schütz, *Wiley Interdiscip. Rev.: Comput. Mol. Sci.*, 2012, **2**, 242.

[47] H.-J. Werner, P. J. Knowles, G. Knizia, F. R. Manby, M. Schütz, P. Celani, W. Györffy, D. Kats, T. Korona, R. Lindh, A. Mitrushenkov, G. Rauhut, K. R. Shamasundar, T. B. Adler, R. D. Amos, A. Bernhardsson, A. Berning, D. L. Cooper, M. J. O. Deegan, A. J. Dobbyn, F. Eckert, E. Goll, C. Hampel, P. Palmieri, D. Peng, K. Pflüger, R. Pitzer, M. Reiher, T. Shiozaki, H. Stoll, A. J. Stone, R. Tarroni, T. Thorsteinsson and M. Wang, *MOLPRO, version 2015.1 a package of ab initio programs*, see http://www.molpro.net, 2015.

[48] X. Zhu and D. R. Yarkony, *J. Chem. Phys.*, 2010, **132**, 104101.

[49] X. Zhu and D. R. Yarkony, *J. Chem. Phys.*, 2012, **136**, 174110.

[50] X. Zhu and D. R. Yarkony, *J. Phys. Chem. A*, 2015, **119**, 12383.

[51] X. Zhu and D. R. Yarkony, *J. Chem. Phys.*, 2016, **144**, 044104.

[52] B. O. Roos, P. R. Taylor and P. E. M. Siegbahn, *Chem. Phys.*, 1980, **48**, 157.

[53] B. O. Roos, *Int. J. Quantum Chem. Symp.*, 1980, **18**, 175.

[54] H.-J. Werner and W. Meyer, *J. Chem. Phys.*, 1981, **74**, 5794.

[55] H.-J. Werner and P. J. Knowles, *J. Chem. Phys.*, 1985, **82**, 5053.

[56] P. J. Knowles and H.-J. Werner, *Chem. Phys. Lett.*, 1985, **115**, 259.

[57] R. Krishnan, J. S. Binkley, R. Seeger and J. A. Pople, *J. Chem. Phys.*, 1980, **72**, 650.

[58] T. Clark, J. Chadrasekhar, G. W. Spitznagel and P. von R. Schleyer, *J. Comp. Chem.*, 1983, **4**, 294.

[59] F. Weigend and R. Ahlrichs, *Phys. Chem. Chem. Phys.*, 2005, **7**, 3297.

[60] P. L. Barbieri, P. A. Fantin and F. E. Jorge, *Mol. Phys.*, 2006, **104**, 2945.

[61] D. Rappoport and F. Furche, *J. Chem. Phys.*, 2010 **133**, 134105.

[62] T. H. Dunning, Jr., *J. Chem. Phys.*, 1989, **90**, 1007.

[63] R. A. Kendall, T. H. Dunning, Jr. and R. J. Harrison, *J. Chem. Phys.*, 1992, **96**, 6796.

[64] E. Papajak, H. R. Leverentz, J. Zheng and D. G. Truhlar, *J. Chem. Theory Comput.*, 2009, **5**, 1197.

[65] E. Papajak, D. G. Truhlar, *J. Chem. Theory Comput.*, 2010, **6**, 567.

[66] K. Andersson, P. A. Malmqvist, B. O. Roos, A. J. Sadlej, K. Wolinski, J. Phys. Chem., 1990, **94**, 5483.

[67] H.-J. Werner, *Mol. Phys.*, 1996, **89**, 645.

[68] J. Finley, P. A. Malmqvist, B. O. Roos, and L. Serrano-Andrés, Chem. Phys. Letters, 1998, 288, 299-306.

[69] T. Shiozaki, W. Győrffy, P. Celani, and H.-J. Werner, *J. Chem. Phys.*, 2011, **135**, 081106.

[70] X. Xu, J. Zheng, K. R. Yang and D. G. Truhlar, *J. Am. Chem. Soc.*, 2014, **136**, 16378.

Table-of-Contents Graphic:
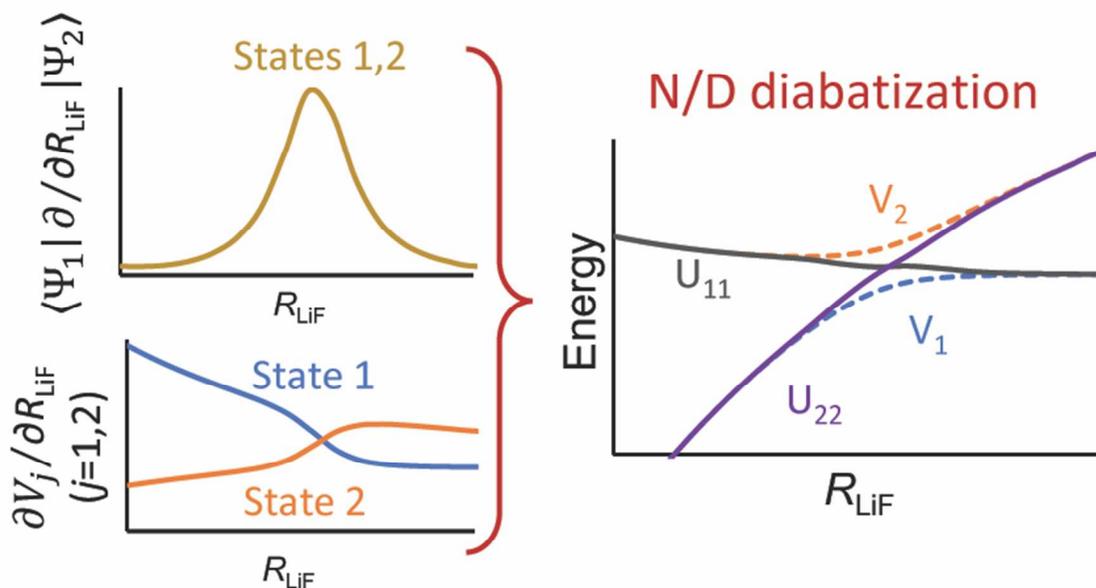


Text to accompany Table-of-Contents Graphic:

We propose a new diabatization method that is direct, orbital-free, and adiabatic-equivalent based on directly calculated nonadiabatic couplings of states and the adiabatic energy gradients.